Title

Shared Mechanisms Govern HIV Transcriptional Suppression in Circulating CD103+ and Gut CD4+ T Cells

Journal

Journal of Virology, 95(2)

ISSN

0022-538X

Authors

Yukl, Steven A
Khan, Shahzada
Chen, Tsui-Hua
et al.

Publication Date

2020-12-22

DOI

10.1128/jvi.01331-20

Peer reviewed

AMERICAN SOCIETY FOR MICROBIOLOGY | Journal of Virology®

GENOME REPLICATION AND REGULATION OF VIRAL GENE EXPRESSION

Shared Mechanisms Govern HIV Transcriptional Suppression in Circulating CD103$^+$ and Gut CD4$^+$ T Cells

Steven A. Yukl,[a,e] Shahzada Khan,[c] Tsui-Hua Chen,[a,b] Martin Trapecar,[c] Frank Wu,[c] Guorui Xie,[c,h] Sushama Telwatte,[a,e] Daniel Fulop,[c] Alexander R. Pico,[c] Gregory M. Laird,[d] Kristen D. Ritter,[d] Norman G. Jones,[e] Chuanyi M. Lu,[a,b] Robert F. Siliciano,[f,g] Nadia R. Roan,[c,h] Jeffrey M. Milush,[e] Ma Somsouk,[i] Steven G. Deeks,[e] Peter W. Hunt,[e] Shomyseh Sanjabi[c,j*]

[a]San Francisco Veterans Affairs Medical Center, San Francisco, California, USA
[b]University of California, San Francisco, San Francisco, California, USA
[c]Gladstone Institutes, San Francisco, California, USA
[d]Accelevir Diagnostics, Baltimore, Maryland, USA
[e]Department of Medicine, University of California, San Francisco, School of Medicine, San Francisco, California, USA
[f]Department of Medicine, Johns Hopkins University School of Medicine, Baltimore, Maryland, USA
[g]Howard Hughes Medical Institute, Baltimore, Maryland, USA
[h]Department of Urology, University of California, San Francisco, San Francisco, California, USA
[i]Division of Gastroenterology, University of California, San Francisco, San Francisco, California, USA
[j]Department of Microbiology and Immunology, University of California, San Francisco, San Francisco, California, USA

Steven A. Yukl and Shahzada Khan contributed equally. Author order was determined by seniority.

ABSTRACT Latent HIV infection is the main barrier to cure, and most HIV-infected cells reside in the gut, where distinct but unknown mechanisms may promote viral latency. Transforming growth factor β (TGF-β), which induces the expression of CD103 on tissue-resident memory T cells, has been implicated in HIV latency. Using CD103 as a surrogate marker to identify cells that have undergone TGF-β signaling, we compared the HIV RNA/DNA contents and cellular transcriptomes of CD103$^+$ and CD103$^-$ CD4 T cells from the blood and rectum of HIV-negative (HIV$^-$) and antiretroviral therapy (ART)-suppressed HIV-positive (HIV$^+$) individuals. Like gut CD4$^+$ T cells, circulating CD103$^+$ cells harbored more HIV DNA than did CD103$^-$ cells but transcribed less HIV RNA per provirus. Circulating CD103$^+$ cells also shared a gene expression profile that is closer to that of gut CD4 T cells than to that of circulating CD103$^-$ cells, with significantly lower expression levels of ribosomal proteins and transcriptional and translational pathways associated with HIV expression but higher expression levels of a subset of genes implicated in suppressing HIV transcription. These findings suggest that blood CD103$^+$ CD4 T cells can serve as a model to study the molecular mechanisms of HIV latency in the gut and reveal new cellular factors that may contribute to HIV latency.

IMPORTANCE The ability of HIV to establish a reversibly silent, "latent" infection is widely regarded as the main barrier to curing HIV. Most HIV-infected cells reside in tissues such as the gut, but it is unclear what mechanisms maintain HIV latency in the blood or gut. We found that circulating CD103$^+$ CD4$^+$ T cells are enriched for HIV-infected cells in a latent-like state. Using RNA sequencing (RNA-seq), we found that CD103$^+$ T cells share a cellular transcriptome that more closely resembles that of CD4$^+$ T cells from the gut, suggesting that they are homing to or from the gut. We also identified the cellular genes whose expression distinguishes gut CD4$^+$ or circulating CD103$^+$ T cells from circulating CD103$^-$ T cells, including some genes that have been implicated in HIV expression. These genes may contribute to latent HIV infection in the gut and may serve as new targets for therapies aimed at curing HIV.

Citation Yukl SA, Khan S, Chen T-H, Trapecar M, Wu F, Xie G, Telwatte S, Fulop D, Pico AR, Laird GM, Ritter KD, Jones NG, Lu CM, Siliciano RF, Roan NR, Milush JM, Somsouk M, Deeks SG, Hunt PW, Sanjabi S. 2021. Shared mechanisms govern HIV transcriptional suppression in circulating CD103$^+$ and gut CD4$^+$ T cells. J Virol 95:e01331-20. https://doi.org/10.1128/JVI.01331-20.

Editor Frank Kirchhoff, Ulm University Medical Center

Address correspondence to Steven A. Yukl, steven.yukl@ucsf.edu, or Shomyseh Sanjabi, Sanjabi.shomyseh@gene.com.

* Present address: Shomyseh Sanjabi, Genentech, South San Francisco, California, USA.

Received 6 July 2020
Accepted 23 October 2020
Accepted manuscript posted online 28 October 2020
Published 22 December 2020

KEYWORDS CD103, CD4 T cell, HIV-1, PD-1, gamma delta T cell, human immunodeficiency virus, intestines, latency, tissue-resident memory cell, transforming growth factor receptors

Latently HIV-infected CD4 T cells, which do not constitutively produce virions but can be induced to produce infectious virus upon activation (1–3), represent the major barrier to HIV cure and may be concentrated in the gut (4–12). Transforming growth factor β (TGF-β) has been implicated in the establishment of HIV latency (13–16), but it is unclear what cell types are susceptible to enhanced HIV latency by TGF-β-mediated mechanisms. TGF-β induces the expression of CD103 (integrin αE) on CD8$^+$ tissue-resident memory cells (TRMs), and the expression of αE(CD103)β7 integrin on TRMs promotes their interaction and retention in the epithelium (17, 18). Most CD8 TRMs in the gut coexpress CD69 and CD103, whereas only a small fraction of CD4 TRMs express CD103 (19). Human CD103$^+$ CD4 T cells have also been described in the blood although at a much lower frequency than what is observed in the gut (20). We hypothesized that CD103$^+$ cells may harbor a higher burden of latent HIV infection.

Programmed cell death 1 (PD-1) has also been associated with HIV latency (21) in circulating CD4$^+$ T cells (22, 23) and lymph node PD-1$^+$ T follicular helper (Tfh) cells (24–26), which are found among CXCR5- and PD-1-expressing cells (25). However, it is unclear whether PD-1$^+$ or Tfh cells from the gut are enriched for latent HIV. Therefore, we measured HIV DNA and RNA levels in CD4 T cells that do or do not express CD103, PD-1, and CXCR5 from the blood and gut of HIV-positive (HIV$^+$) antiretroviral therapy (ART)-treated participants. We found that circulating CD103$^+$ cells resemble gut memory CD4 T cells in that they are highly enriched for HIV DNA but show very low baseline levels of HIV transcription per provirus. Since most proviruses are defective (27), and even cells with infectious proviruses cannot always be induced by activation (28), we used the "intact provirus DNA assay" (IPDA) (29) and a modification of the viral outgrowth assay to show that a subset of these circulating CD103$^+$ T cells contains proviruses that are likely infectious and can be induced by activation to produce supernatant virus. Using RNA sequencing (RNA-seq), we found that these circulating CD103$^+$ T cells are transcriptionally closer to gut memory CD4 T cells than to CD103$^-$ cells from blood. We identified shared cellular genes in circulating CD103$^+$ and gut CD4 T cells that likely contribute to the suppression of HIV transcription and a latent-like HIV infection. Our findings suggest that CD103$^+$ CD4 T cells in blood could serve as a surrogate cell type to study the molecular mechanism of HIV latency in the gut and identify potential targets for new therapies aimed at disrupting latent HIV infection.

RESULTS

A subset of memory CD4$^+$ T cells in blood and gut expresses CD103 irrespective of HIV status. To investigate the localization of CD4$^+$ CD103$^+$ T cells in gut tissues, immunohistochemistry was performed on biopsy specimens from the ileum and rectosigmoid of two HIV-negative (HIV$^-$) donors. As expected, most CD103$^+$ CD3$^+$ cells were CD8$^+$ and located in the intraepithelial layer of rectal tissue (Fig. 1a and b). CD4$^+$ cells were predominantly found in the lamina propria, and only a minority, which were located near the epithelium, expressed CD103 (Fig. 1a and b).

Flow cytometry was used to measure the frequencies of CD4$^+$ CD103$^+$ cells in peripheral blood mononuclear cells (PBMCs) and rectosigmoid biopsy specimens collected from 6 HIV$^-$ and 20 HIV$^+$ donors (Table 1). Since HIV infection can downregulate CD4 expression on T cells (30), CD4 T cells were quantified by gating on the CD3$^+$ CD8$^-$ population (Fig. 1c). Most T cells in the rectosigmoid biopsy specimens were CD45RA$^-$ memory T cells, and most of the CD103$^+$ T cells were also CD69$^+$, suggesting that these are likely TRMs, whereas most CD103$^+$ T cells in the peripheral blood were CD69$^-$ (Fig. 1c). In blood, the average proportion of CD3$^+$ CD45RA$^-$ CD8$^-$ memory cells that were CD103$^+$ was significantly lower in HIV$^+$ than in HIV$^-$ individuals (Fig. 1d), although the proportions of CD3$^+$ CD45RA$^-$ CD8$^+$ T cells that were CD103$^+$ did not significantly differ by HIV infection status (Fig. 1e). We also gated on CD3$^+$ CD45RA$^-$ CD4$^+$ memory

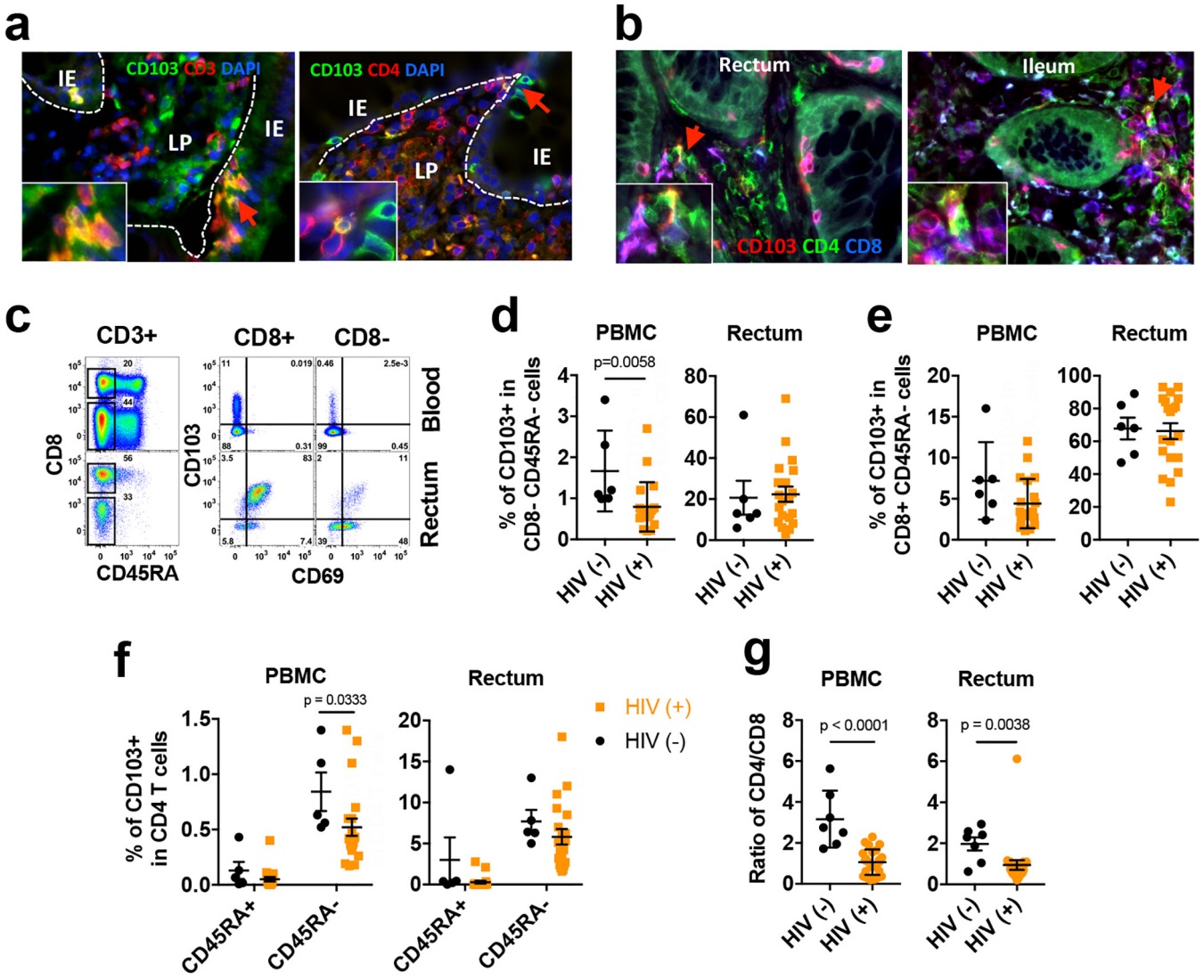

FIG 1 A small subset of tissue-resident CD4+ T cells expresses CD103. (a) Immunohistochemical detection of CD103 (green), CD3 (red), and DNA (blue) in rectosigmoid tissue. IE, intraepithelial region; LP, lamina propria. (b) Immunohistochemical detection of CD103 (red), CD4 (green), and CD8 (blue) in the indicated tissues. (c) Representative flow cytometry plots showing the abundances of CD8+/− and CD45RA-negative cells among CD3+ populations in blood and rectal biopsy specimens (left) and the abundances of T cells positive for CD103 and/or CD69 among CD8-positive or -negative populations in blood and rectal biopsy specimens (right). (d) Frequency of CD103+ CD8− CD45RA− memory CD3+ cells among PBMCs or rectal cells in HIV+ and HIV− individuals. (e) Frequency of CD103+ CD8+ CD45RA− memory CD3+ cells among PBMCs or rectal cells in HIV+ and HIV− individuals. (f) Frequency of CD103+ cells among CD45RA+ and CD45RA− CD4 T cells within PBMCs or the rectum of HIV+ or HIV− individuals. (g) Ratio of CD4 T cells to CD8 T cells among PBMCs or rectum samples from HIV+ or HIV− individuals. Data represent results from 1 of 2 (a and b) or 1 of 6 (c) HIV− donors or from 6 HIV− and 20 HIV+ donors (d to g). Statistical differences between HIV+ and HIV− individuals were assessed using the Mann-Whitney U test (d to g).

T cells and similarly found that the proportion of CD103+ cells was low in the blood of HIV+ compared to HIV− participants (Fig. 1f). In the rectosigmoid, the proportions of CD103+ CD8−, CD103+ CD4+, and CD103+ CD8+ memory T cells were comparable between the HIV− and HIV+ groups (Fig. 1d to f). As expected, the ratios of CD4+ to CD8+ T cells in both blood and rectal tissues were significantly lower in HIV+ than in HIV− individuals (Fig. 1g). These observations confirmed that despite their low frequency, CD103+ CD4+ memory T cells are detectable in the blood and gut of HIV− and ART-treated HIV+ individuals.

Mass cytometry by time-of-flight (CyTOF) was used to further characterize the phenotypic properties of CD103+ and CD103− T cells from blood and rectal biopsy specimens from two ART-suppressed, HIV+ participants (Table 1). CD4 T cells were initially defined by gating on live CD3+ CD8− cells, followed by gating on the CD45RA+

TABLE 1 Characteristics of HIV$^+$ and HIV$^-$ donors[a]

Patient ID	HIV status	VL (log_{10} copies/ml)	CD4 count (cells/mm^3)	Sex	Age (yrs)	Time on ART (yrs)	Figure(s)
1997	HIV$^-$	<40	435	M	56	NA	Fig. 1c to g, Fig. 4
1852	HIV$^-$	ND	1,490	M	38	NA	Fig. 1c to g, Fig. 4
6590	HIV$^-$	ND	665	F	64	NA	Fig. 1c to g, Fig. 4
6593	HIV$^-$	ND	635	M	57	NA	Fig. 1c to g, Fig. 4, 7, and 8
6506	HIV$^-$	<40	525	M	40	NA	Fig. 1c to g, Fig. 4, 7, and 8
6532	HIV$^-$	<40	969	M	61	NA	Fig. 1c to g, Fig. 4, 7, and 8
1788	HIV$^+$	331	1,063	M	51	1	Fig. 1c to g, Fig. 3
3162	HIV$^+$	<40	847	M	55	21	Fig. 1c to g, Fig. 3
1195	HIV$^+$	<40	702	M	55	7	Fig. 1c to g, Fig. 3
3025	HIV$^+$	<40	478	M	58	20	Fig. 1c to g, Fig. 3
1644	HIV$^+$	<40	247	M	54	8	Fig. 1c to g, Fig. 3
7269	HIV$^+$	<40	226	M	66	3	Fig. 1c to g, Fig. 3
2475	HIV$^+$	<40	568	M	56	12	Fig. 1c to g, Fig. 3
1710	HIV$^+$	<40	696	M	60	6	Fig. 1c to g, Fig. 3
2754	HIV$^+$	<40	658	M	37	2	Fig. 1c to g, Fig. 3
2347	HIV$^+$	<40	409	M	65	19	Fig. 1c to g, Fig. 3
7251	HIV$^+$	<40	673	M	54	5	Fig. 1c to g, Fig. 3
2403	HIV$^+$	<40	1,170	M	54	19	Fig. 1c to g, Fig. 3
2027	HIV$^+$	<40	592	M	61	20	Fig. 4 and 5
1631	HIV$^+$	<40	768	M	48	8	Fig. 4 and 5
1181	HIV$^+$	<40	716	F	62	12	Fig. 4 and 5
3147	HIV$^+$	<40	682	M	60	24	Fig. 4 and 5
2447	HIV$^+$	<40	785	F	56	12	Fig. 4
1380	HIV$^+$	<40	838	F	58	8	Fig. 4
1570	HIV$^+$	<40	484	M	57	9	Fig. 4, 7, and 8
2151	HIV$^+$	<40	1,119	M	61	15	Fig. 4, 7, and 8
2643	HIV$^+$	<40	816	M	55	2	Fig. 4, 7, and 8
S3	HIV$^+$	184	878	F	53	14	Fig. 2
S4	HIV$^+$	50	682	F	45	19	Fig. 2
2511	HIV$^+$	<40	357	M	50	8	Fig. 6
2125	HIV$^+$	<40	807	M	52	14	Fig. 6
3171	HIV$^+$	<40	232	M	65	16	Fig. 6

[a]ND, not done; NA, not applicable; VL, viral load; M, male; F, Female. Gray shading separates subsets of study participants used in different figures.

CD103$^-$ population that is enriched for naive T cells and the CD45RA$^-$ CD103$^+$ and CD45RA$^-$ CD103$^-$ memory populations (Fig. 2a). As an alternative to defining CD4 T cells as CD8$^-$, we also gated live CD3$^+$ cells as CD4$^+$, followed by gating on the CD45RA$^+$ CD103$^-$ population and the memory CD45RA$^-$ CD103$^+$ and CD45RA$^-$ CD103$^-$ populations (Fig. 2b). While a number of differences were observed between CD45RA$^-$ CD3$^+$ CD8$^-$ CD103$^+$ and CD103$^-$ memory cells in the rectum (Fig. 2a), the majority of these differences were no longer observed when we specifically gated on CD3$^+$ CD4$^+$ T cells, except for slightly higher expression levels of PD-1, ICOS, CCR7, and CD38 in the CD103$^-$ fraction. In contrast, both gating strategies revealed differences between the CD103$^+$ and CD103$^-$ T cells from blood. Interestingly, the low expression level of CD127 and the high expression levels of CD25 and cytotoxic-T lymphocyte-associated antigen 4 (CTLA4) in the blood CD103$^+$ fractions suggest that these cells may be enriched for regulatory T (Treg) cells (Fig. 2a and b). In both the blood and rectum, CD103$^-$ CD4 T cells tended to show higher expression levels of CXCR5, suggesting the inclusion of follicle-homing T cells in this population (Fig. 2a and b). For comparison, we also characterized the expression levels of all the markers on CD3$^+$ CD8$^+$ T cells from the rectum and blood (Fig. 2c). Together, data from this analysis suggest that while there are major phenotypic differences between CD45RA$^+$ and CD45RA$^-$ cells in both the rectum and blood, the phenotypic differences between CD3$^+$ CD4$^+$ CD103$^+$ and CD3$^+$ CD4$^+$ CD103$^-$ cells in the rectum are minimal. In contrast, more phenotypic differences are observed among the CD3$^+$ CD4$^+$ CD103$^+$ and CD3$^+$ CD4$^+$ CD103$^-$ cells in the blood.

Circulating CD103$^+$ T cells are as enriched for HIV DNA as rectal CD4 T cells. To investigate whether cells expressing Tfh markers (CXCR5 and PD-1) or CD103 are enriched for latent HIV infection, we first used fluorescence-activated cell sorter (FACS)

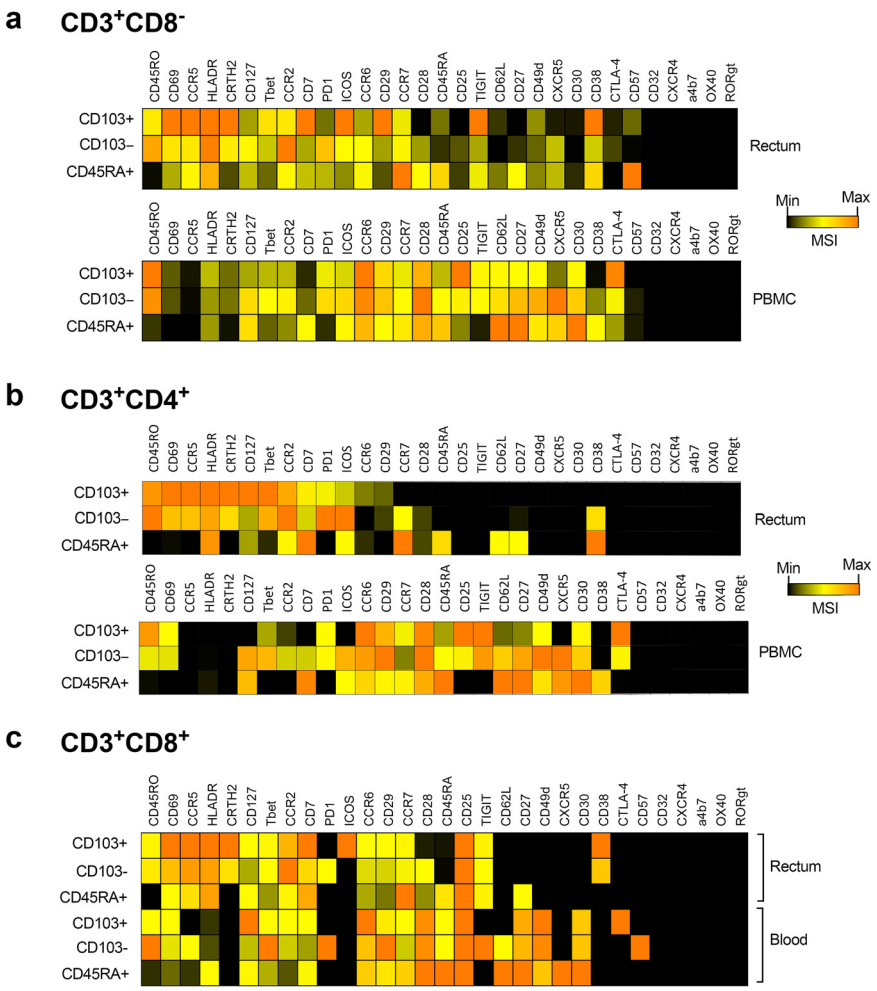

FIG 2 CyTOF reveals differences in expression between CD103$^+$ and CD103$^-$ T cells. Cells from the rectum (top of each panel) and PBMCs (bottom of each panel) from two HIV$^+$ ART-suppressed individuals were analyzed by mass cytometry. Live CD3$^+$ T cells were gated into CD8$^-$ (a), CD4$^+$ (b), or CD8$^+$ (c) populations and then further separated into CD45RA$^+$ (naive), CD45RA$^-$ CD103$^+$, or CD45RA$^-$ CD103$^-$ populations. Shown are heat map comparisons of mean signal intensities (MSIs) in each population.

analysis to sort CD3$^+$ CD8$^-$ CD45RA$^-$ T cells from the blood and rectum of 12 ART-suppressed individuals (Table 1) into 4 populations: (i) CXCR5$^+$ PD-1$^{+/-}$ (enriched for Tfh), (ii) CD103$^+$ PD-1$^-$, (iii) CD103$^+$ PD-1$^+$, and (iv) CD103$^-$ PD-1$^{+/-}$ (Fig. 3a). In the blood, the CD103$^+$ PD-1$^+$ cells (0.06% of CD3$^+$ cells) and CD103$^+$ PD-1$^-$ cells (0.16% of CD3$^+$ cells) were present at lower frequencies than the other two sorted populations (Fig. 3b and c). In rectal biopsy specimens, CD103$^+$ PD-1$^+$ cells were the least abundant (1.63%), followed by CXCR5$^+$ (6.14%), CD103$^+$ PD-1$^-$ (6.2%), and CD103$^-$ (29.98%) cells (Fig. 3b and c).

Total HIV DNA was measured in each population using droplet digital PCR (ddPCR) (Fig. 3d). In the blood, total HIV DNA levels per 10^6 cells (normalized by copies of the human gene telomere reverse transcriptase [TERT]) were significantly higher in both CD103$^+$ populations than in either the CD103$^-$ population (median [CD103$^+$ PD-1$^-$/CD103$^-$] = 8.6 [$P = 0.0049$]; median [CD103$^+$ PD-1$^+$/CD103$^-$] = 8.4 [$P = 0.0015$]) or the CXCR5$^+$ population (median [CD103$^+$ PD-1$^-$/CXCR5$^+$] = 6.7 [$P = 0.0093$]; median [CD103$^+$ PD-1$^+$/CXCR5$^+$] = 10.8 [$P = 0.0068$]) (Fig. 3d).

In the rectum, no statistically significant difference was observed between HIV DNA levels in any of the memory populations, although the CD103$^+$ PD-1$^-$ fraction tended to have less HIV DNA (Fig. 3d). HIV DNA levels in the rectal CXCR5$^+$ and CD103$^-$ T cells were higher than those in the corresponding populations in the blood (median ratios

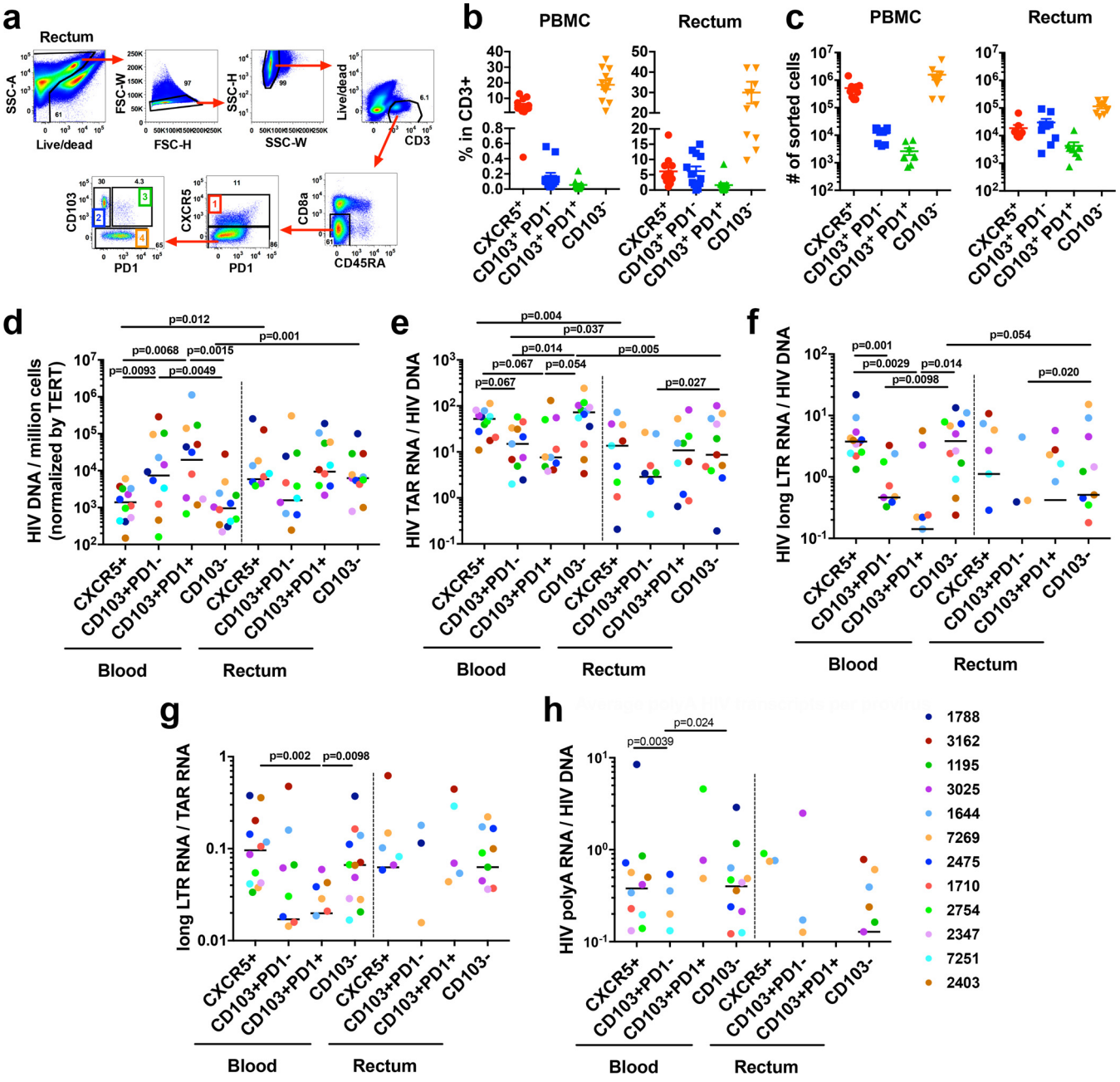

FIG 3 Blood CD103$^+$ CD8$^-$ T cells are enriched for HIV DNA but transcribe less HIV RNA per provirus. To determine the comparative HIV burdens in individual cell types, we FACS isolated CXCR5$^+$, CD103$^+$ PD-1$^-$, CD103$^+$ PD-1$^+$, and CD103$^-$ T cells from both PBMCs and rectosigmoid biopsy specimens of 12 ART-suppressed individuals and measured HIV DNA and HIV transcription by ddPCR. (a) Gating strategy for cell sorting. SSC, side scatter; FSC, forward scatter. (b) Frequency of sorted cells among CD3$^+$ lymphocytes from PBMCs and rectal biopsy specimens. (c) Total number of sorted cells. (d to h) HIV levels in sorted populations from blood and rectum. (d) HIV DNA copies per million cells in each population. (e) Total initiated (TAR) HIV transcripts per provirus. (f) 5′-elongated (long-LTR) transcripts per provirus. (g) Ratio of 5′-elongated to initiated HIV transcripts. (h) Polyadenylated HIV transcripts per provirus. Differences between cell populations in HIV levels (d to h) were assessed in a pairwise fashion using the Wilcoxon signed-rank test.

of 3.6 and 4.2 [$P = 0.012$ and $P = 0.001$, respectively]), while HIV DNA levels in the CD103$^+$ PD-1$^+$ and CD103$^+$ PD-1$^-$ populations did not differ between the blood and rectum (Fig. 3d; see also Fig. S1 in the supplemental material). Qualitatively similar findings were observed regardless of the method of normalization to cell numbers (measured TERT versus sort counts), treatment of samples with no detectable HIV DNA (zero versus no value), or the exclusion of samples with <5 positive droplets (Fig. S2a to c). Collectively, these data demonstrate that blood CD103$^+$ cells are enriched for HIV

DNA to a degree similar to those of CXCR5$^+$, CD103$^+$ PD-1$^+$, and CD103$^-$ CD4 T cells from the gut.

Circulating CD103$^+$ T cells transcribe less HIV RNA per provirus. To quantify progression through various stages of HIV transcription in each cell type, we used recently developed reverse transcription (RT)-ddPCR assays (31, 32) to quantify the levels of total (initiated [TAR region]), 5′-elongated (R-U5-pre-Gag ["long-LTR" {elongated long terminal repeat}]), and polyadenylated {U3-poly(A) ["poly(A)"]} HIV RNAs in each of the 4 FACS-sorted populations of CD3$^+$ CD8$^-$ CD45RA$^-$ T cells from the blood and gut (Fig. 3e to h). HIV RNA levels were expressed as copies per 10^6 cells by levels of TERT and then further normalized by HIV DNA copies per 10^6 cells to calculate the average levels per provirus of initiated, elongated, and polyadenylated HIV transcripts.

In the blood, the level of HIV transcriptional initiation (TAR RNA/HIV DNA) tended to be lower in both CD103$^+$ populations than in either the CD103$^-$ population (median [CD103$^+$ PD-1$^-$/CD103$^-$] = 0.19 [$P = 0.014$]; median [CD103$^+$ PD-1$^+$/CD103$^-$] = 0.10 [$P = 0.054$]) or the CXCR5$^+$ population (median [CD103$^+$ PD-1$^-$/CXCR5$^+$] = 0.29 [$P = 0.067$]; median [CD103$^+$ PD-1$^+$/CXCR5$^+$] = 0.21 [$P = 0.067$]) (Fig. 3e). In the rectum, the level of HIV transcriptional initiation was lower in CD103$^+$ PD-1$^-$ than in CD103$^-$ cells ($P = 0.027$), but otherwise, we did not detect differences between rectal populations in levels of HIV transcriptional initiation (Fig. 3e). The level of HIV transcriptional initiation was also lower in the rectal CXCR5$^+$, CD103$^+$ PD-1$^-$, and CD103$^-$ cells than in the corresponding populations in the blood (median ratios = 0.23, 0.17, and 0.33, respectively [$P = 0.004$, 0.037, and 0.005, respectively]) (Fig. 3e; Fig. S1), while no difference was observed between blood and rectal CD103$^+$ PD-1$^+$ fractions ($P = 0.50$). Similar findings were observed when the analysis was limited to samples with both detectable HIV RNA and DNA (Fig. S2d), suggesting that the low levels of HIV transcriptional initiation in the circulating CD103$^+$ cells (compared to CD103$^-$ cells) and in the rectal CD103$^-$ cells (compared to blood) are not solely explained by a lack of detectable HIV RNA in samples with lower cell numbers.

Even more pronounced differences were observed in the levels of 5′-elongated HIV transcripts (long-LTR) per provirus. Among the 12 participants, elongated HIV transcripts were detectable in blood CD103$^+$ PD-1$^-$ cells from 8 individuals and CD103$^+$ PD-1$^+$ cells from 6 individuals, compared to all 12 individuals for CXCR5$^+$ and CD103$^-$ cell populations. In the blood, levels of elongated HIV transcripts per provirus were lower in both CD103$^+$ populations than in either the CD103$^-$ cells (median [CD103$^+$ PD-1$^-$/CD103$^-$] = 0.093 [$P = 0.0098$]; median [CD103$^+$ PD-1$^+$/CD103$^-$] = 0.013 [$P = 0.014$]) or the CXCR5$^+$ cells (median [CD103$^+$ PD-1$^-$/CXCR5$^+$] = 0.11 [$P = 0.001$]; median [CD103$^+$ PD-1$^+$/CXCR5$^+$] = 0.015 [$P = 0.0029$]) (Fig. 3f). In the rectum, the level of elongated HIV RNA/provirus was lower in the CD103$^+$ PD-1$^-$ than in the CD103$^-$ cells ($P = 0.020$), but no other significant differences were observed between populations. Levels of elongated HIV RNA/provirus also tended to be lower in rectal CD103$^-$ cells than in blood CD103$^-$ cells (median ratio = 0.55 [$P = 0.054$]) (Fig. 3f; Fig. S1). Similar findings were observed when the analysis was limited to samples with both detectable HIV RNA and DNA (Fig. S2e).

To measure the degree of HIV transcriptional elongation, we calculated the ratio of 5′-elongated to initiated HIV RNA transcripts in each population. In the blood, the ratio of elongated/total HIV RNA was lower in the CD103$^+$ PD-1$^+$ population than in either the CD103$^-$ cells (median [CD103$^+$ PD-1$^+$/CD103$^-$] = 0.13 [$P = 0.0098$]) or the CXCR5$^+$ cells (median [CD103$^+$ PD-1$^+$/CXCR5$^+$] = 0.14 [$P = 0.002$]) (Fig. 3g).

Polyadenylated HIV RNA was infrequently detected in either CD103$^+$ population. In the blood, the level of polyadenylated HIV RNA was lower in the CD103$^+$ PD-1$^-$ population than in either the CXCR5$^+$ or CD103$^-$ populations ($P = 0.0039$ and $P = 0.024$, respectively), but no other significant differences were observed (Fig. 3h; S2f). No significant difference in HIV DNA content (Fig. 3d) or HIV transcription per provirus (Fig. 3e, f, and h) was observed between blood CD103$^+$ T cells (either PD-1$^+$ or PD-1$^-$) and either rectal CXCR5$^+$, CD103$^+$ PD-1$^+$, or CD103$^-$ T cells, suggesting that

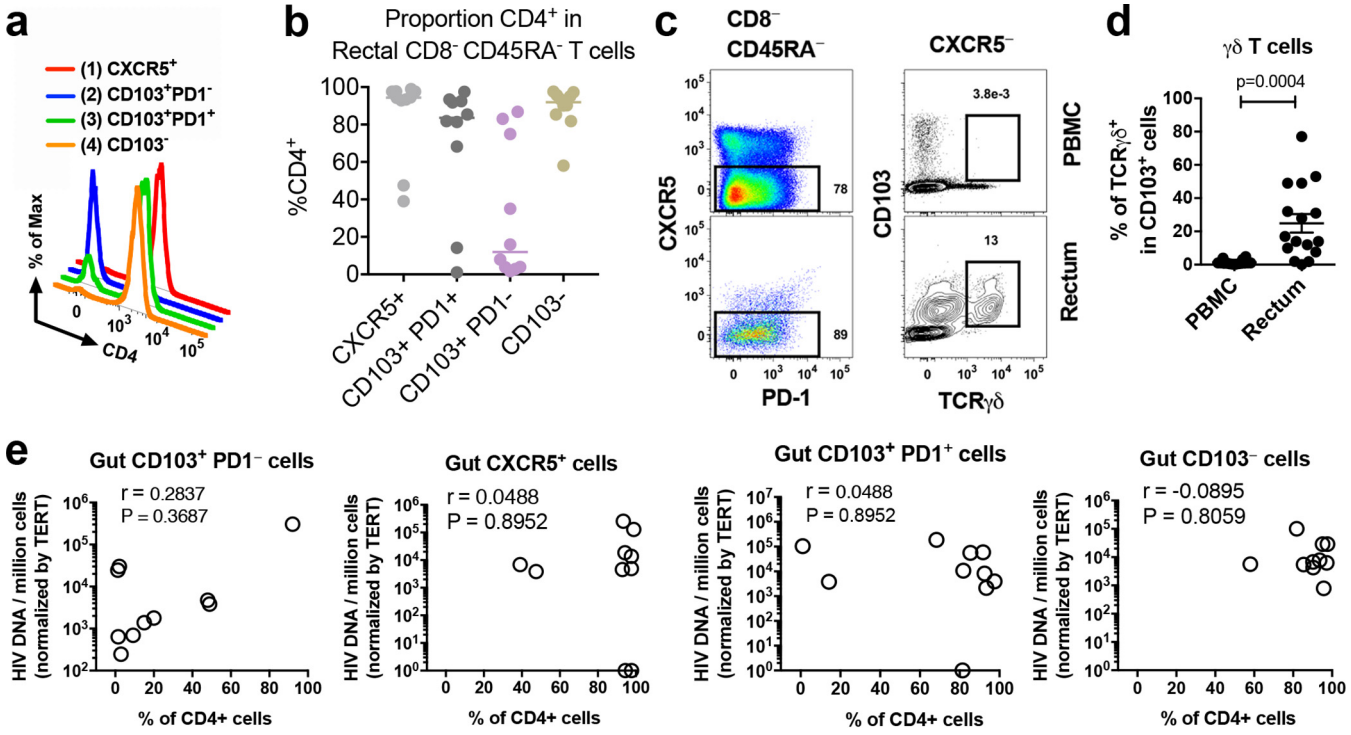

FIG 4 The rectal CD103$^+$ PD-1$^-$ population has a high frequency of CD4$^-$ γδ T cells. (a) Representative histogram showing the expression of CD4 among rectal CXCR5$^+$, CD103$^+$ PD-1$^-$, CD103$^+$ PD-1$^+$, and CD103$^-$ populations. (b) Percentage of each rectal cell population expressing CD4. (c) To determine whether the rectal CD103$^+$ PD-1$^-$ cells that did not express CD4 were γδ T cells, the flow cytometry panel was modified to include antibodies to the TCRγδ. Representative flow plots depict the frequency of CD103$^+$ TCRγδ$^+$ cells in blood and rectum. (d) Frequency of γδ T cells in rectal biopsy specimens and PBMCs. Significance was determined using the Wilcoxon signed-rank test. (e) Correlation between HIV DNA copies per million cells and the proportion of CD4$^+$ T cells in each rectal population. *P* and *r* values are from Spearman correlations.

the blood CD103$^+$ T cells resemble these three populations of rectal CD4$^+$ T cells in HIV infection frequency and viral transcriptional activity.

A fraction of CD103$^+$ PD-1$^-$ cells in the gut consists of γδ T cells. A large fraction of the CD8$^-$ CD103$^+$ PD-1$^-$ population in the rectal biopsy specimens did not express CD4, whereas most cells from all other rectal populations and all blood populations expressed CD4 (Fig. 4a and b). Since gut CD3$^+$ cells could include Vδ2$^+$ gamma delta (γδ) T cells, which also express CD103, we modified our flow panel to include antibodies to T cell receptor γδ (TCRγδ) and measured the frequency of γδ T cells among CD3$^+$ CD45RA$^-$ CD8$^-$ CD103$^+$ cells (Fig. 4c and d). The frequency of γδ T cells was higher in rectal biopsy specimens than in blood (mean, 24.8% versus 1.4% [$P = 0.0004$]) (Fig. 4c and d). Although peripheral Vγ9Vδ2 T cells can harbor latent HIV (33), their contribution to the HIV burden in gut tissue is largely unknown. To determine whether HIV DNA levels varied with the relative proportions of CD4$^-$ γδ T cells versus CD4$^+$ T cells in the rectal CD103$^+$ PD-1$^-$ population, we assessed the correlation between HIV DNA and the percentage of CD4$^+$ cells (Fig. 4e) in all rectal populations. HIV DNA levels correlated closely with the percentage of CD4$^+$ cells in the rectal CD103$^+$ PD-1$^-$ population ($R^2 = 0.60$ [$P = 0.003$ by linear regression analysis]; $r = 0.28$ [$P =$ NS {not significant} by Spearman correlation]) compared to other cell populations ($P =$ NS by any method) (Fig. 4e), suggesting that more HIV DNA is present in CD4$^+$ than in γδ T cells in the rectal biopsy specimens. Because γδ T cells also comprised a small fraction (mean, 1.4%) of blood CD8$^-$ CD103$^+$ cells (Fig. 4c), a new gating strategy (Fig. 5a) was implemented to separate γδ T cells from CD4$^+$ T cells and to sort CD4$^+$ T cells into more pure populations of Tfh-like cells (defined as CXCR5$^+$ PD-1^{hi}) and CD4$^+$ T cells that do or do not express CD103 (irrespective of PD-1).

Gamma delta T cells and CD103$^+$ CD4$^+$ T cells may transcribe less HIV. In order to measure HIV levels in more pure populations of γδ T cells, Tfh cells, and CD103$^+$

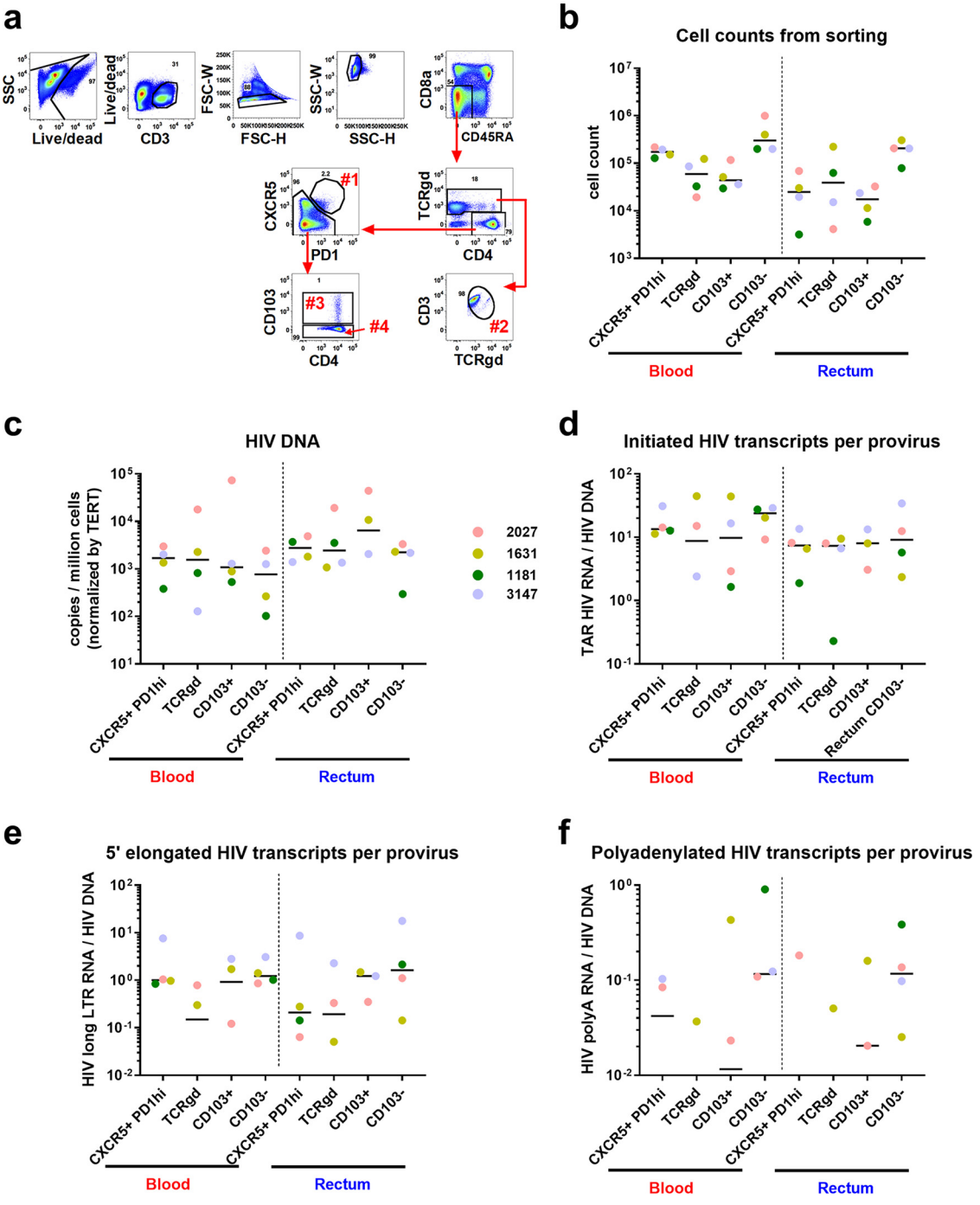

FIG 5 HIV persists in gamma delta T cells and CD103+ CD4+ T cells from the blood and rectum. To determine the comparative HIV burdens in more pure populations of γδ T cells, Tfh-like cells, and CD103+ CD4+ T cells, blood and rectal cells from 4 additional ART-suppressed individuals were sorted into TCRγδ T cells, CD4+ CXCR5+ PD-1hi cells, CD4+ CD103+ T cells, and CD103− CD4+ T cells. (a) Gating strategy for cell sorting. (b) Total number of sorted cells. (c to f) HIV levels in sorted populations from blood and rectum. (c) HIV DNA copies per million cells in each population. (d) Total initiated (TAR) HIV transcripts per provirus. (e) 5′-elongated (long-LTR) transcripts per provirus. (f) Polyadenylated HIV transcripts per provirus.

CD4+ T cells, we recruited four additional ART-suppressed study participants and used the revised gating strategy (Fig. 5a) to sort cells from the blood and rectum into 4 new populations: (i) CD3+ CD8− CD45RA− TCRγδ+ (γδ T), (ii) CD3+ CD8− CD45RA− CD4+ CXCR5+ PD-1hi (Tfh-like), (iii) CD3+ CD8− CD45RA− CD4+ CD103+ (CD103+ CD4+ T), and (iv) CD3+ CD8− CD45RA− CD4+ CD103− (CD103− CD4+ T).

HIV DNA and levels of initiated, 5′-elongated, and polyadenylated HIV transcripts were measured in each population using ddPCR (Fig. 5b to e). HIV DNA was detected in $\gamma\delta$ T cells from the blood and rectum in 4 of 4 individuals (Fig. 5b). In all four individuals, HIV DNA levels were higher in circulating Tfh-like and CD103$^+$ CD4$^+$ T cells than in CD103$^-$ CD4$^+$ T cells, although the small number of study participants precluded finding statistically significant differences (P = NS). In accord with the above-described results using the first gating scheme, the median levels per provirus of 5′-elongated and polyadenylated HIV transcripts tended to be lower in circulating $\gamma\delta$ T cells and CD103$^+$ CD4$^+$ T cells (3 to 4 out of 4 individuals) than in CD103$^-$ CD4$^+$ T cells (Fig. 5d and e) (P = NS).

Circulating CD103$^+$ CD4 T cells contain intact proviruses. To determine whether the circulating CD103$^+$ T cells contain proviruses that are likely to be infectious, we used a recently described duplex ddPCR assay (the IPDA) that distinguishes defective proviruses from those that are likely to be intact (29). Levels of total, 5′-defective, 3′-defective, and "intact" proviruses were measured in four populations of FACS-sorted cells from leukapheresis samples from 3 HIV$^+$ ART-suppressed individuals: (i) CD3$^+$ CD8$^-$ CD45RA$^-$ TCR$\gamma\delta^+$ (TCR$\gamma\delta^+$), (ii) CD3$^+$ CD8$^-$ CD45RA$^-$ CD4$^+$ CXCR5$^+$ PD-1^{hi} (Tfh-like), (iii) CD3$^+$ CD8$^-$ CD45RA$^-$ CD4$^+$ CD103$^+$ (CD103$^+$), and (iv) CD3$^+$ CD8$^-$ CD45RA$^-$ CD4$^+$ CD103$^-$ (CD103$^-$) cells. Circulating CD103$^+$ cells from all participants contained intact proviruses, although they did not appear to be particularly enriched for them (Fig. 6a and b).

Circulating CD103$^+$ CD4 T cells can be induced *ex vivo* to produce HIV RNA. To determine the degree to which the greater block to HIV transcription in CD103$^+$ cells could be reversed by T cell activation *ex vivo*, we performed a modification of the viral outgrowth assay (3) using CXCR5$^+$ PD-1^{hi} (Tfh-like), CD103$^+$, and CD103$^-$ populations sorted from leukapheresis samples from 3 ART-suppressed individuals. Significantly more CD103$^-$ cells were available for testing (Fig. 6c). The sorted cells were cultured with anti-CD3/anti-CD28 beads plus phytohemagglutinin (PHA)-activated CD4$^+$ T cells from 2 HIV$^-$ donors, and HIV RNA was measured in cell-free supernatants. Supernatant HIV RNA could be detected in the activated CD103$^+$ and Tfh-like cells from 2 out of 3 individuals, compared to 3/3 for the CD103$^-$ cells (Fig. 6d to f). In one patient for whom the sort yield of each cell population was high enough for replicate terminal dilutions, the estimated frequency of cells that could be induced to produce supernatant HIV RNA was 2.0×10^{-6} (5% to 95%, 5×10^{-7} to 8.2×10^{-6}) in the CD103$^+$ cells, versus 3.4×10^{-6} (1.4×10^{-6} to 8.3×10^{-6}) for CD103$^-$ cells and $>4.2 \times 10^{-6}$ (5%, 3.3×10^{-6}) for Tfh-like cells (Fig. 6f). These findings suggest that the proviruses in some circulating CD103$^+$ cells can be induced by T cell activation to produce supernatant virus.

HIV-mediated gene expression changes are observed only in blood CD103$^-$ cells. To gain further insight into how blood CD103$^+$ and gut CD4$^+$ T cells maintain HIV in a transcriptionally silent state, RNA sequencing was performed on sorted CD103$^+$ and CD103$^-$ CD4$^+$ T cells (Fig. 5a) from paired blood and colon biopsy specimens from 3 HIV$^+$ and 3 HIV$^-$ donors. To determine whether ART-treated HIV infection affects gene expression, we compared the transcriptomes of cells isolated from HIV$^+$ and HIV$^-$ individuals. Differential expression between HIV$^+$ and HIV$^-$ individuals was observed only in the blood CD103$^-$ population, where only 2 genes, NKG7 and zinc finger 431 (ZNF431), showed different transcript levels (Fig. 7a; Table S1). No significant differences were observed between HIV$^+$ and HIV$^-$ individuals in the transcriptomes from blood CD103$^+$ (Table S2) or gut CD103$^-$ (Table S3) or CD103$^+$ (Table S4) cells. These data suggest that ART-treated participants have minimal HIV-mediated changes in host transcriptional activity in these memory T cell subsets.

Blood CD103$^+$ cells share a subset of their transcriptome with gut cells. To assess how HIV transcriptional activity is differentially regulated in the blood and gut CD103$^-$ and CD103$^+$ CD4 T cells, we next examined global gene expression in each cellular subset. Since HIV status did not alter the transcriptome profiles (except for the

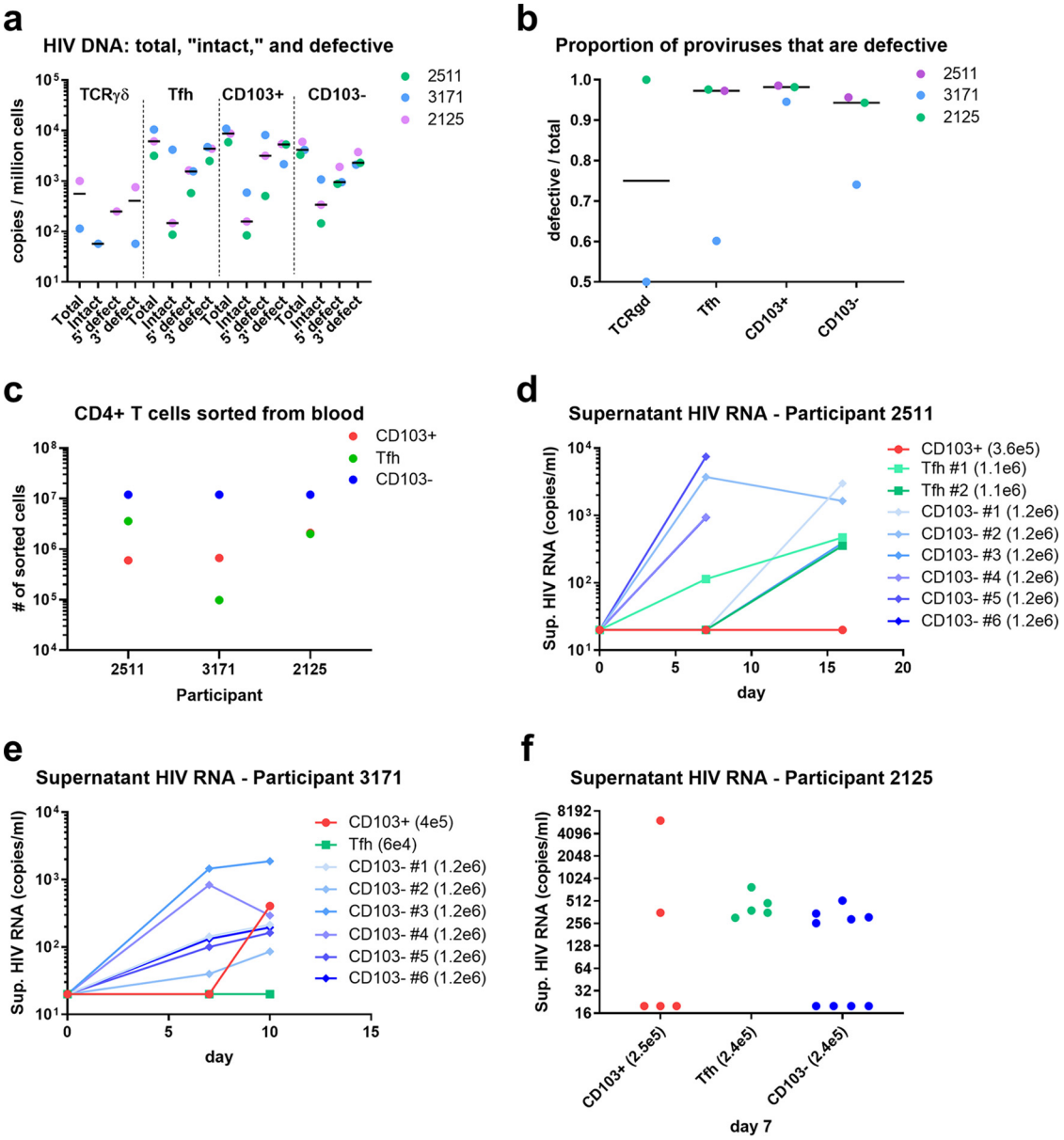

FIG 6 CD103+ CD4+ T cells from blood contain some intact proviruses and can be induced by activation to produce viral genomic RNA in the supernatant. (a) Copies per million cells of total, 5′-defective, 3′-defective, and likely intact proviruses in each sorted cell type, as measured by ddPCR using the intact proviral DNA assay. (b) Ratio of defective (5′ and 3′) to total proviruses in each cell type. Intact proviruses were not detectable in the γδ T cell population from one donor. (c) Number of total sorted cells for the activation-induced HIV RNA production assay. (d) Supernatant HIV RNA (*y* axis) (measured by the Abbott RealTime assay) over time (*x* axis) after *ex vivo* activation and coculture of sorted CD103+ (red), CXCR5+ PD-1hi (green), and CD103− (blue) CD4 T cells from blood of 3 ART-suppressed individuals. For the first two individuals (patients 2511 and 3171), up to 1.2×10^6 sorted cells (or the maximum number of cells available, which was lower for the CD103+ fraction) were cultured with 1.2×10^6 activated cells from each of two donors. Values in parentheses indicate the number of patient cells in each well and replicate; the number of CD103+ cells was insufficient for replicates. For the 3rd patient (2125), for whom yields of sorted CD103+ and CXCR5+ PD-1hi cells were higher, each cell type was cultured in replicates (dots) at the same cell number.

two genes mentioned above), we combined the transcriptomics data from HIV+ and HIV− samples. When the transcriptomes of CD103+ CD4 T cells from the rectum and blood were compared, over 3,000 differentially expressed genes (DEGs) were identified (Fig. 7b; Table S5), with enrichment of genes associated with tissue residency in cells isolated from the rectal biopsy specimens (Table S5). In contrast, a comparison between CD103+ and CD103− CD4 T cells isolated from rectal biopsy specimens revealed only 6 DEGs, including ITGAE, which encodes the αE subunit of CD103 (Fig. 7c; Table S6). The

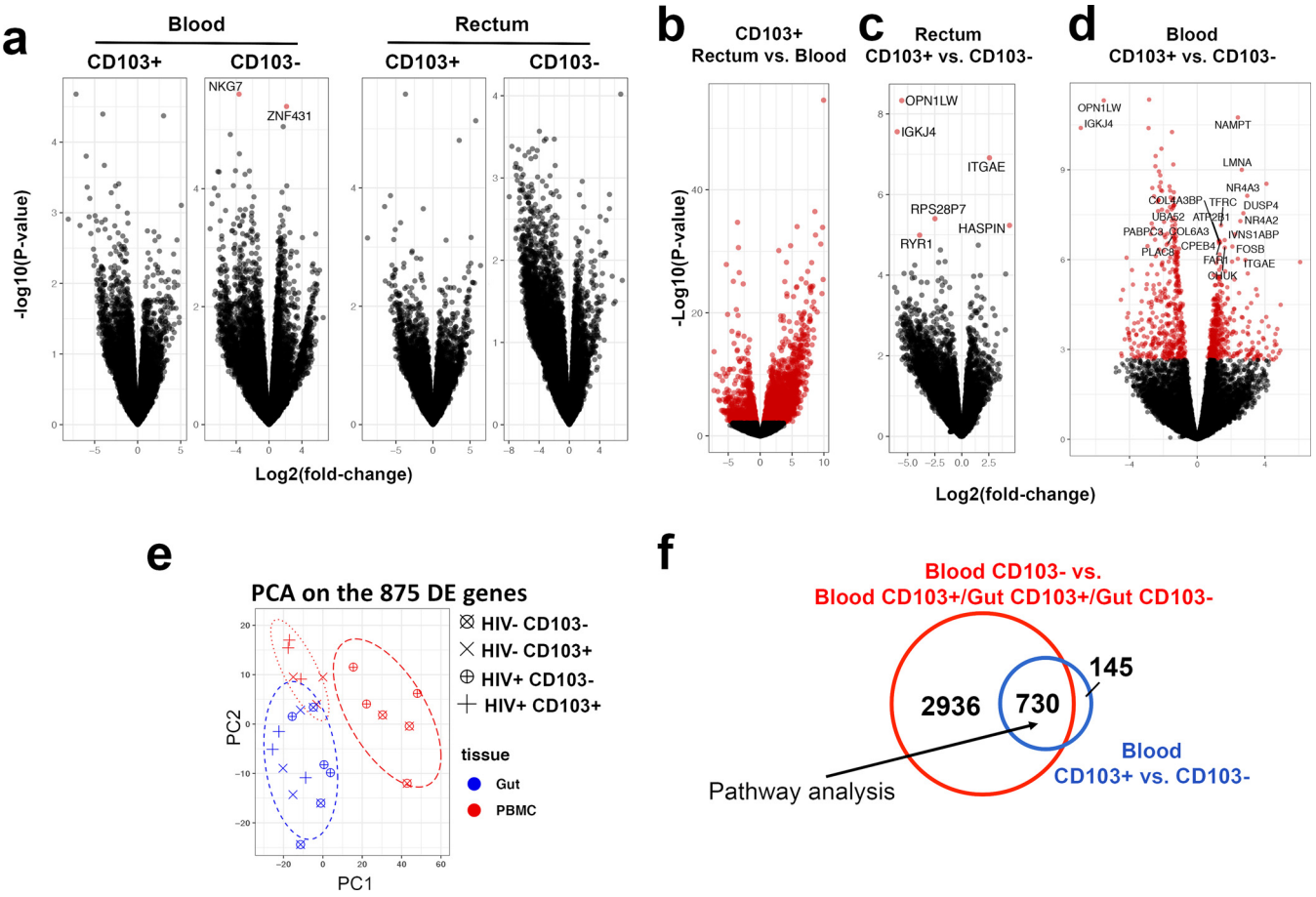

FIG 7 Circulating CD103$^+$ CD4$^+$ T cells show a transcriptome that overlaps those of CD103$^+$ and CD103$^-$ CD4$^+$ T cells from the gut. To determine the similarities in transcriptome profiles between CD103$^+$ and CD103$^-$ populations from the blood and rectum, we combined the transcriptomics data from HIV$^+$ and HIV$^-$ samples. (a) Volcano plot representation of differential gene expression between CD103$^+$ and CD103$^-$ populations in the blood and rectum. (b) Volcano plot representation of differentially expressed genes between the rectum and blood in CD103$^+$ cells. (c) Volcano plot representation of differentially expressed genes between CD103$^+$ and CD103$^-$ populations in the rectum. (d) Volcano plot representation of differentially expressed genes between CD103$^+$ and CD103$^-$ populations in the blood. (e) Principal-component analysis (PCA) of differentially expressed (DE) genes (DEGs) in different cell populations of HIV$^+$ and HIV$^-$ rectal and blood samples. (f) Venn diagram indicating the number of shared and uniquely expressed genes comparing blood CD103$^-$ to CD103$^+$ cells (blue) or blood CD103$^-$ to the combination of blood CD103$^+$ and gut CD103$^{+/-}$ T cells (red). Data represent results from 3 HIV$^-$ and 3 HIV$^+$ donors. See Fig. 5a for the gating strategy, and see Tables S1 to S8 in the supplemental material for lists of DEGs.

low numbers of DEGs between gut CD103$^+$ and gut CD103$^-$ cells suggest that they are very similar to one another.

In contrast, 875 DEGs were identified between blood CD103$^+$ and blood CD103$^-$ CD4 T cells (Fig. 7d; Table S7), suggesting that although both are circulating, these cellular subsets have significantly different transcriptomes. Principal-component (PC) analysis of these 875 genes across all cell types showed that the blood CD103$^+$ cells clustered between gut cells and blood CD103$^-$ cells (Fig. 7e), suggesting transcriptomic overlap and potential similarities between blood CD103$^+$ and gut T cells. To further evaluate this overlap, we created a Venn diagram of these 875 genes and the genes differentially expressed in blood CD103$^-$ compared to all other cells; 730 overlapping genes were identified (Fig. 7f; Tables S7 and S8), again showing that the blood CD103$^+$ cells resemble gut cells in regard to the expression of this subset of genes.

Blood CD103$^+$ T cells and gut T cells differ from blood CD103$^-$ T cells in the expression of distinct pathways and ribosomal proteins. To investigate how blood CD103$^+$ and gut CD4 T cells maintain HIV in a less transcriptionally active state, we performed pathway analysis on the 730 genes differentially expressed between CD103$^-$ and blood CD103$^+$/gut cells to determine which pathways and biological processes are enriched in this gene set. Pathways with very high combined scores

belonged to cytoplasmic ribosomal proteins, signal recognition particle (SRP)-dependent cotranslational proteins, and viral transcription (Fig. 8a, top). Other pathways with lower combined scores included mRNA processing, regulation of transcription, phosphorylation of RNA polymerase II (Pol II), TGF-β signaling, glucocorticoid receptor signaling, RNA splicing, hypertrophy model, DNA damage response, aryl hydrocarbon receptor, circadian rhythm, mitogen-activated protein kinase (MAPK) signaling, and interleukin-1 (IL-1) signaling pathways (Fig. 8a, bottom). Unsupervised clustering of the samples based on the annotated genes among these 730 DEGs clustered the blood CD103$^+$ cells closer to the gut cells, while the blood CD103$^-$ cells clustered separately from all other cells (Fig. 8b). Notably, almost one-fourth of the DEGs belonged to ribosomal proteins, which are expressed at lower levels in blood CD103$^+$ and gut cells than in blood CD103$^-$ cells (Fig. 8b).

CORUM analysis, which detects mammalian protein complexes, identified two complexes that contain these downregulated ribosomal proteins: the Nop56p-associated pre-rRNA complex (Fig. 8c) and the HIV-1 TAR RNA binding protein (TRBP) complex (Fig. 8d) (34), which can increase HIV expression and replication by inhibiting the interferon (IFN)-induced protein kinase PKR (35) and by increasing the translation of HIV mRNA (36). In contrast, a cluster of genes belonging to the spliceosome complex (Fig. 8e) and accessory genes involved in mRNA processing (Fig. S3a) were significantly upregulated in the blood CD103$^+$ and gut cells, while genes encoding some of the proteins in respiratory chain complex I (Fig. 8f) and complexes IV and V (Fig. S3b) were downregulated. This pattern of low mRNA expression levels of ribosomal proteins and respiratory chain complexes in blood CD103$^+$ and gut T cells has been associated with T cells that are in a more quiescent state (37–39).

Link between low expression levels of ribosomal proteins and other differentially expressed genes. It is possible that differences in cellular gene expression in blood CD103$^+$ and gut CD4 T cells, including low expression levels of ribosomal proteins, lead to HIV transcriptional silencing due to a low abundance of factors that are needed to induce viral transcription. Therefore, STRING analysis was performed to determine how the low expression levels of ribosomal proteins would affect the expression of other potentially relevant genes (Fig. 8g). We found that upregulation of the most significant DEGs in blood CD103$^+$ compared to blood CD103$^-$ cells (Fig. 7d), namely, NAMPT, LMNA, NR4A3, and NR4A2, can be linked to the low expression levels of ribosomal proteins and, as discussed below, can directly inhibit HIV transcription.

DISCUSSION

Since CD103 may mark a subtype of tissue-resident or tissue-homing cells that have undergone TGF-β signaling, we hypothesized that CD103$^+$ CD4 T cells are more likely to maintain HIV in a transcriptionally repressed, latent state. Because PD-1 has also been associated with HIV latency in circulating CD4$^+$ T cells (21–23) and lymph node PD-1$^+$ or CXCR5$^+$ PD-1$^+$ Tfh cells (25, 26), we compared the levels of HIV DNA and different HIV transcripts in T cells from the blood and gut that do or do not express various combinations of CD103, CXCR5, and PD-1.

CD103 expression was detected on a proportion of memory CD4$^+$ T cells from the gut. These CD103$^+$ gut cells likely represent a subset of tissue-resident memory (TRM) CD4$^+$ T cells, since CD103 promotes cell retention in the epithelium (17), and these cells also express high levels of CD69, which is used as a marker for TRM cells (19). CD103 is also expressed by regulatory T (Treg) cells (40), and TGF-β signaling is known to be important for the differentiation of both Treg and Th17 cells (41), both of which have been reported to harbor higher levels of HIV DNA (42–45). However, the gut CD103$^+$ T cells do not appear to be either Treg or Th17 cells. Based on our CyTOF analysis, the rectal CD103$^+$ CD4$^+$ cells expressed medium to high levels of CD127 (which is not typical of Treg cells) and did not express other markers expected in Treg cells (CD25, CTLA4, Ox40, and CD62L) (Fig. 2a and b) (40, 46). The rectal CD103$^+$ cells expressed low levels of CCR6 (Fig. 2a and b), which is usually expressed at high levels on Th17 cells and has been associated with higher HIV DNA levels in blood and rectal cells (42–45). They

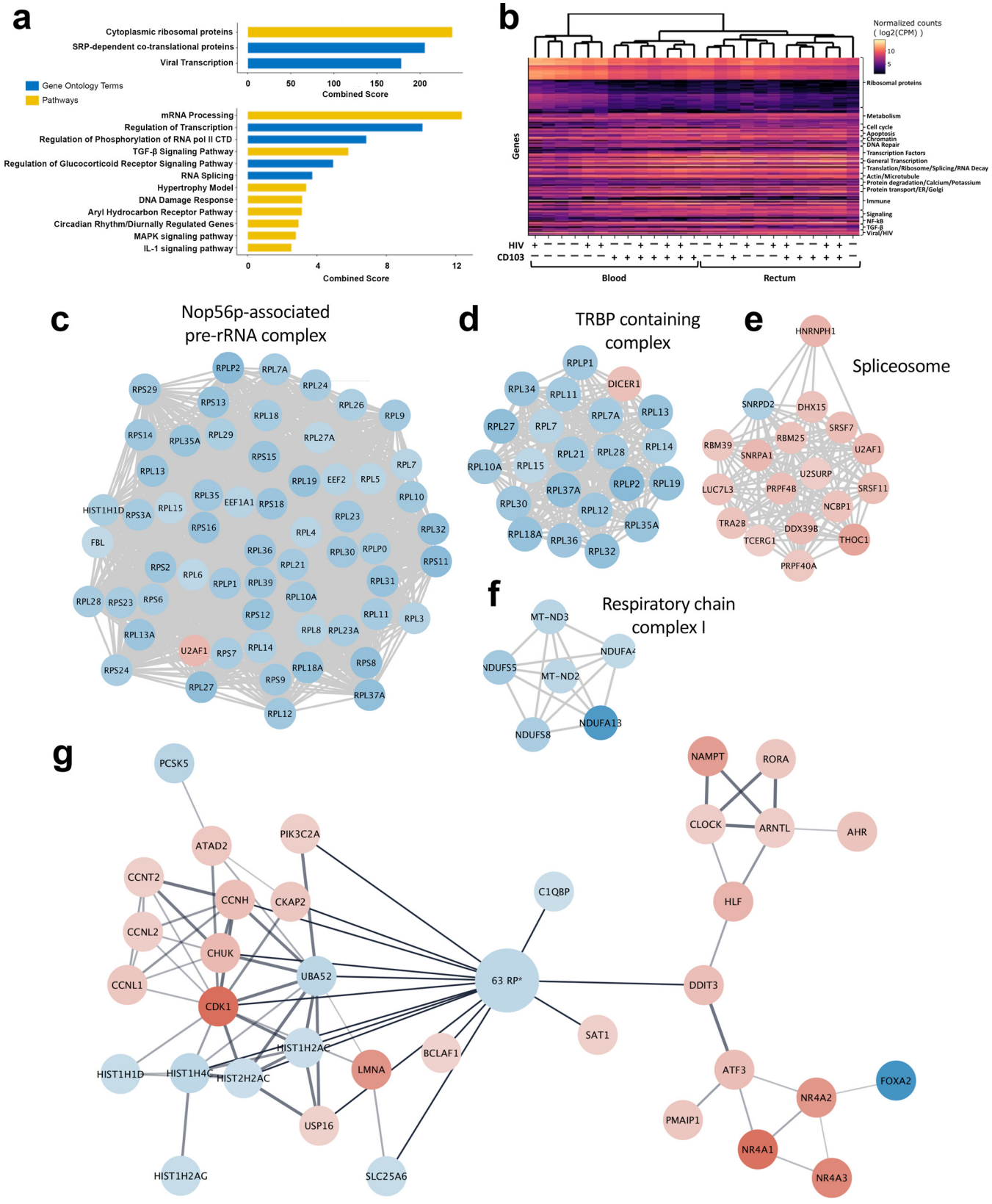

FIG 8 CD103$^+$ blood T cells resemble gut T cells in the differential expression of genes involved in transcription, translation, signaling, and metabolism. Shown is a functional characterization of DEGs shared between blood and gut CD103$^+$ populations. (a) Pathway and Gene Ontology terms ranked by combined scores from enrichment analysis. CTD, C-terminal domain. (b) Unsupervised clustering of the samples based on the annotated genes among shared DEGs. ER, endoplasmic reticulum; CPM, counts per million. (c to f) CORUM analysis identifies mammalian protein complexes (red, upregulated; blue, downregulated). (g)

(Continued on next page)

also did not express RORγt, a transcription factor driving Th17 differentiation. Therefore, the rectal CD103$^+$ CD4 T cells do not appear to represent a pure population of either Treg or Th17 cells.

We did not detect a significant difference in HIV DNA levels between rectal CD103$^-$ cells and either the rectal CD103$^+$ PD-1$^+$ or CD103$^+$ PD-1$^-$ populations. One explanation is that the gut CD103$^+$ and CD103$^-$ CD4$^+$ T cells are phenotypically similar, as suggested by our CyTOF and transcriptomic studies. Since TGF-β levels are higher in the gut, it is possible that even the CD103$^-$ gut cells have been exposed to TGF-β. CD103$^-$ CD4$^+$ rectal cells also expressed high levels of CD69, suggesting that most of them are tissue-resident memory cells.

HIV DNA levels were approximately 4-fold higher in the rectal CXCR5$^+$ and CD103$^-$ T cells than in their counterparts in the blood, in accord with previous studies suggesting higher levels of HIV DNA per million CD4$^+$ T cells in the gut than in the blood (7, 8, 11). These findings are also in accord with a recent report that tissue-resident CD4$^+$ T cells from the cervix harbor HIV DNA at levels higher than those in blood CD4 T cells (47).

In the gut, we did not find a significant difference in HIV DNA between the Tfh-enriched (CXCR5$^+$) cells and the three CXCR5$^-$ populations, which appears to contrast with previous reports of higher HIV DNA levels in PD-1$^+$ and PD-1$^+$ CXCR5$^+$ Tfh cells from lymph nodes (25, 26). However, when we specifically sorted the CXCR5$^+$ PD-1^{hi} cells (which likely constitute a purer population of Tfh cells), the median HIV DNA level tended to be higher in the circulating Tfh-like population than in the non-Tfh, CD103$^-$ population. Future studies using more individuals will be needed to determine whether these CXCR5$^+$ PD-1^{hi} cells have other features of Tfh cells and whether they are enriched for HIV DNA in the blood or rectum.

CD103 expression was also detected on a small subset of T cells in the blood, which showed some phenotypic differences from CD103$^+$ cells in the gut. For example, CD103$^+$ CD4$^+$ T cells from the blood expressed less CD69 than did CD103$^+$ T cells from the rectum (Fig. 2a and b). The blood CD103$^+$ CD4$^+$ T cells showed some features of Treg cells (CD103^{hi}, CD25^{hi}, CTLA4^{hi}, and CD127^{low}), suggesting that they might be enriched for Treg cells, although they did not express Ox40 (Fig. 2a and b) (40, 46). They expressed high levels of CCR6 (which could be consistent with Th17) but did not express RORγt, suggesting that they are probably not Th17 cells. In contrast to the gut, where HIV DNA levels were not significantly higher in CD103$^+$ than in CD103$^-$ cells, both PD-1$^+$ and PD-1$^-$ populations of circulating CD103$^+$ cells were highly enriched for HIV DNA (approximately 8-fold) compared to either the circulating CD103$^-$ or CXCR5$^+$ populations. HIV DNA levels in the blood CD103$^+$ cells were also similar to those in CXCR5$^+$, CD103$^+$ PD-1$^+$, and CD103$^-$ T cells from the gut. Given the similarities in HIV DNA levels and gene expression levels between blood CD103$^+$ cells and CD103$^+$ or CD103$^-$ CD4 T cells in the gut, it is possible that similar factors contribute to either preferential infection or proliferation/survival of these cell types.

HIV DNA was also detected in rectal CD103$^+$ PD-1$^-$ T cells (which contain a significant proportion of $\gamma\delta$ T cells) and in sorted $\gamma\delta$ T cells from both the blood and rectum. HIV DNA has previously been detected in circulating $\gamma\delta$ T cells (33), but our observation extends this finding to the gut, where we found that $\gamma\delta$ T cells constitute a higher proportion of CD3$^+$ cells. We also detected intact HIV DNA in circulating $\gamma\delta$ T cells from some individuals, suggesting that $\gamma\delta$ T cells can be reservoirs for infectious HIV (33).

In agreement with previous studies showing less HIV transcriptional initiation in the rectum (biopsy specimens or sorted CD4 T cells) than in the blood (PBMCs or sorted CD4 T cells) (31), we found that the levels per provirus of total (initiated) and 5′-

FIG 8 Legend (Continued)
Network reconstruction of enriched ontology terms (red, upregulated; blue, downregulated). RP*, ribosomal protein. See also Fig. S3 in the supplemental material for affected genes in enriched pathways.

elongated HIV transcripts tended to be lower in the rectal CXCR5$^+$ and CD103$^-$ T cells than in their counterparts in the blood. The lower HIV transcription levels in the gut may seem paradoxical since one might imagine that exposure to gut microbial products would increase immune activation (especially with the increase in gut permeability observed with HIV infection) (48), which can stimulate HIV transcription. In addition, the frequency of T cells that express markers of "activation" (such as the combination of CD38 and HLA-DR) is higher in the gut than in the blood in both HIV$^+$ (8) and HIV$^-$ (49) individuals. However, it is likely that the gut immune system has evolved mechanisms of tolerance to microbial products from the normal flora. For example, gut macrophages differ from monocytes and *in vitro*-differentiated macrophages in that most do not express CD14, which serves as a receptor for lipopolysaccharide (LPS) (50). Likewise, our RNA-seq data showed profound differences in cellular gene transcription between gut T cells and their circulating counterparts. These differences in host gene expression may render gut T cells less responsive to microbial products from the normal flora and/or reduce constitutive HIV transcription, even in cells that express nonspecific surface markers associated with activation.

As predicted by the study hypothesis, CD103$^+$ cells from the blood showed lower levels of initiated and elongated HIV transcripts per provirus than either the CXCR5$^+$ or the CD103$^-$ cells from the blood. The difference was more pronounced for elongated transcripts, and CD103$^+$ cells also showed a lower ratio of elongated to initiated HIV transcripts, indicating that the expression of CD103 in blood cells is associated with a stronger block to HIV transcriptional elongation. The levels per provirus of initiated and elongated HIV transcripts in these circulating CD103$^+$ T cells were comparable to those in rectal CXCR5$^+$, CD103$^+$ PD-1$^+$, and CD103$^-$ T cells, which is in accord with their overlap in cellular gene transcription and suggests that similar mechanisms may reduce HIV transcription in these cell types.

Levels per provirus of initiated and elongated HIV transcripts were also lower in the rectal CD103$^+$ PD-1$^-$ T cells (which contain more $\gamma\delta$ T cells) than in the rectal CD103$^-$ cells. In the blood, the median levels per provirus of 5′-elongated and polyadenylated transcripts also tended to be lower in sorted $\gamma\delta$ T cells than in CD103$^-$ CD4$^+$ T cells. These findings suggest that $\gamma\delta$ T cells may also harbor mechanisms that suppress HIV transcription, although future studies with more participants are needed to confirm this observation.

Since most proviruses are defective, and some proviral defects (such as those in the LTRs or Tat) could affect HIV transcription, we employed a recently developed assay to measure the levels of "likely intact" and defective proviruses in sorted CD103$^+$, CD103$^-$, Tfh-like, and $\gamma\delta$ T cells from blood. We found that CD103$^+$ CD4$^+$ T cells from blood harbored proviruses that are likely to be intact, although they do not appear to be particularly enriched for intact proviruses. The frequency of defective proviruses may have been slightly higher in the CD103$^+$ than in the CD103$^-$ cells, but with leukapheresis samples from only 3 participants, we were not able to determine whether these differences were statistically significant. Even if there were small differences in the proportions of proviruses with deletions and/or hypermutations in Gag and Env, which may not affect transcription, these minimal differences do not seem to account for the 10-fold differences between CD103$^+$ and CD103$^-$ cells in the levels of elongated HIV transcripts. Instead, it seems likely that the lower levels of HIV transcription in the CD103$^+$ cells reflect specific cellular factors, such as those induced by TGF-β signaling, that inhibit HIV expression.

To further exclude defects that prevent virus production and determine whether the stronger blocks to HIV transcription in CD103$^+$ cells can be reversed by activation, we employed a modification of the coculture assay that is used to quantify latently infected cells (3). We showed that circulating CD103$^+$ cells from 2 of 3 patients could be induced by activation to produce supernatant virus, and in one patient, the frequency of cells that could be induced to produce supernatant virus was similar in CD103$^+$ and CD103$^-$ cells. These findings suggest that the greater blocks to HIV transcriptional initiation and

elongation in CD103$^+$ cells can be reversed by strong T cell-activating stimuli and that some CD103$^+$ cells harbor HIV in an inducible "latent"-like state.

To investigate the relationship between CD103$^+$ and CD103$^-$ T cell populations in the blood and gut and the cellular factors that may contribute to repressing HIV transcription in gut T cells and circulating CD103$^+$ T cells, we applied RNA-seq to CD103$^+$ and CD103$^-$ populations of CD4$^+$ T cells from the blood and gut of HIV-infected and uninfected participants. Differences between HIV$^+$ and HIV$^-$ participants were observed only for blood CD103$^-$ T cells, for which we identified only 2 differentially expressed genes: NKG7 and ZNF431. NKG7 is expressed in the membrane of activated T cells, while ZNF431 is a zinc finger protein that represses cellular transcription by recruiting histone deacetylase 1 (HDAC1) and HDAC2. Since the majority of the CD4 T cells are HIV uninfected, these transcriptional changes in the CD103$^-$ blood cells may be due to the high susceptibility of these cells to bystander effects of an HIV-induced inflammatory environment compared to the gut CD4 T cells or blood CD103$^+$ cells that may be more protected from these environmental cues. Alternatively, these transcriptional changes may be due to the presence of small amounts of viral proteins in a fraction of the blood CD103$^-$ population that may impact host gene transcription. The relationship between the expression of these genes and HIV infection deserves further investigation.

Only six genes were differentially expressed between CD103$^+$ and CD103$^-$ T cells from the gut (one was ITGAE, which encodes CD103), indicating that these cells are transcriptionally very similar. In contrast, 875 genes were differentially expressed between blood CD103$^-$ and CD103$^+$ cells. Many of these genes (730) were also differentially expressed between blood CD103$^-$ and gut T cells, and unsupervised clustering showed that the blood CD103$^+$ T cells were more closely related to gut cells than to blood CD103$^-$ cells. Given their similarities in cellular gene expression, HIV infection frequencies, and HIV transcription levels, it is possible that the blood CD103$^+$ T cells are related to gut cells. Indeed, it was recently reported that human CD4$^+$ CD103$^+$ cutaneous resident memory T cells can be found in the circulation of healthy individuals (20), suggesting that these CD103$^+$ cells are likely TRMs that have entered the circulation.

Pathway analysis of the 730 genes whose expression distinguishes blood CD103$^-$ cells from both blood CD103$^+$ and gut CD103$^{+/-}$ T cells identified ribosomal and cotranslational pathways (which could affect the translation of HIV RNA) and the DNA damage pathway (which could impact HIV integration). We also identified other pathways that can affect HIV transcription, including those implicated in viral transcription, regulation of cellular transcription, phosphorylation of RNA polymerase II (which likely impacts HIV transcriptional elongation) (51), mRNA processing, RNA splicing, circadian rhythm (which has been linked to HIV transcription) (52), and TGF-β (as expected).

Based on the CORUM analysis of protein complexes, we found that blood CD103$^+$ and gut cells showed lower expression levels of the HIV TAR RNA binding protein complex (which could reduce HIV transcription and translation) and differential expression of the tumor necrosis factor alpha (TNF-α)/NF-κB signaling complex (which could reduce HIV transcription in response to TNF-α or T cell activation). Blood CD103$^+$ T cells and gut cells also showed low expression levels of ribosomal proteins and members of the electron transport chain, which have been associated with T cell quiescence (37–39). The more "quiescent" state and lower expression levels of ribosomal proteins in blood CD103$^+$ and gut T cells could contribute to lower levels of translation of HIV RNA as well as lower expression levels of cellular factors necessary for HIV transcription.

Nicotinamide phosphoribosyltransferase (NAMPT) was one of the most significantly upregulated genes in blood CD103$^+$ compared to CD103$^-$ cells and was also significantly more highly expressed in gut than in blood CD4 T cells. NAMPT is the rate-limiting enzyme that adds NAD to sirtuin-1 (SIRT1) to promote its activity (53). Activated SIRT1 can deacetylate p65 (54), which minimizes p65-mediated immune activation, including HIV transcription (55). The downregulation of NAMPT by the microRNA

miR-182 has also been shown to result in Tat-induced LTR transactivation (56). Thus, in the presence of high levels of NAMPT, as is the case in blood CD103$^+$ and gut cells, SIRT1 is likely more active and able to inhibit NF-κB activity, thereby minimizing HIV transcription.

The next most significantly overexpressed gene in CD103$^+$ blood cells is Lamin A/C (LMNA). It was recently shown that Lamin A/C interaction with SUN2 represses chromatin structure and HIV transcription through a reversible mechanism (57). Thus, a high expression level of Lamin A/C in CD103$^+$ blood and gut cells may provide a heightened chromatin block to promote the silencing of the provirus.

The NR4A family of transcription repressors, NR4A1 (Nur77), NR4A2 (NURR1), and NR4A3 (NOR1), was recently shown to be enriched in dysfunctional CD8 T cells and repress effector programs by being recruited to the AP-1 binding sites and inhibiting their transcriptional function (58, 59). Intriguingly, the AP-1 site upstream of the NF-κB element in the HIV promoter has been linked to the ability of HIV to establish latency (60). It is thus tempting to hypothesize that the binding of NR4A molecules to this AP-1 element in the HIV promoter may also contribute to maintaining HIV in a transcriptionally silent state in blood CD103$^+$ and gut CD4$^+$ T cells.

Given the similarities between circulating CD103$^+$ T cells and gut CD4 T cells in HIV DNA levels, HIV transcription, and cellular gene expression, the circulating CD103$^+$ cells described in our study may serve as a surrogate means to understand the mechanisms that enrich for HIV infection and latency in the gut. While gut T cells can be obtained by endoscopic biopsies, it is more difficult, invasive, and time-consuming to obtain gut tissue than to obtain blood. In addition, blood yields more cells with higher viability and is easier and less expensive to process or sort. Although CD103$^+$ T cells constitute a very small proportion of circulating T cells, total CD4$^+$ T cells also represent a small fraction of all gut cells ($\sim$2%) (8, 11, 49). Using only a fraction of the PBMCs available from leukapheresis, we were able to sort more CD103$^+$ CD4 T cells (3×10^5 to $>10^6$) than the total number of CD4$^+$ T cells that can be sorted from 20 gut biopsy specimens (31).

We chose CD103 because it facilitates retention in the gut epithelium and is also induced by TGF-β, which has been suggested to promote HIV latency. However, since gut CD4 T cells in general seem to transcribe less HIV than those in the blood (suggesting that more of them are latently infected), it is possible that other gut homing markers (such as $\alpha 4\beta 7$ and CCR9) may also mark cells that are more likely to be latently infected. Future studies should investigate HIV and cellular gene transcription in blood and gut cells that express these other homing markers. Alternatively, TGF-β could be used *in vitro* to promote HIV latency. For example, one recent article described a primary cell model of HIV latency in which TGF-β is used along with IL-7 to promote T cell survival/quiescence and viral latency in HIV-infected primary CD4 T cells (15).

Limitations of this study should be noted. Given the difficulty in obtaining gut cells from humans, relatively low numbers of study participants were analyzed, which could impair the statistical power to detect significant differences between cell types. The low frequency of some cell populations (CD103$^+$) and low yield of sorted cells can create imprecision in the measurement of HIV DNA and RNA levels, although HIV DNA was almost always detected even in the least abundant CD103$^+$ cells, and similar findings were obtained even when we excluded samples with undetectable HIV DNA or low numbers of HIV-infected cells. While our RNA assays can quantify various blocks to HIV transcription, we are unable to tell how much of each of the HIV RNAs is coming from defective or infectious proviruses. We quantified likely intact proviruses by duplex ddPCR and the ability to induce supernatant HIV RNA in culture, but the numbers of sorted CD103$^+$ cells were deemed insufficient for single-genome nearly full-length proviral sequencing or quantitative viral outgrowth assays. We also used RNA-seq to investigate the cellular factors that may be responsible for suppressing HIV transcription in blood CD103$^+$ and gut CD4 T cells, but the numbers of these cells were not sufficient to measure protein levels or validate these factors using knockdown exper-

iments, so future studies are needed to confirm the contribution of these factors to latent HIV infection.

In summary, we identified a new population of CD103$^+$ CD4$^+$ T cells in the blood that is highly enriched for HIV DNA that is transcriptionally repressed but includes intact proviruses and proviruses that can be induced to produce supernatant HIV RNA upon *ex vivo* stimulation. These circulating CD103$^+$ T cells resemble CD4$^+$ T cells from the gut in their HIV levels and transcriptomes, and they may represent cells that have recirculated from the gut and thus share similar mechanisms of viral latency. Additionally, we identified a number of genes, pathways, and protein complexes whose differential expression is shared between circulating CD103$^+$ T cells and CD4 T cells from the gut and which distinguish them from circulating CD103$^-$ T cells. Therefore, circulating CD103$^+$ cells may represent a more accessible means of studying latent HIV infection in the gut, and their differentially expressed genes may represent new targets for understanding the molecular mechanisms underlying HIV latency and reactivation.

MATERIALS AND METHODS

Study participants. Venous blood, leukapheresis, and gut biopsy specimens were obtained from individuals enrolled in the SCOPE cohort at the University of California, San Francisco (UCSF).

Ethics statement. All protocols (including protocol numbers 10-01218, 10-00263, and 11-07551) were approved by the Committee on Human Research (CHR), the Institutional Review Board (IRB) of UCSF. All study participants provided written informed consent and were adults. All samples were collected at Zuckerberg San Francisco General Hospital and Trauma Center (SFGH) and were anonymized.

Intestinal biopsy specimens. Rectosigmoid (and in some cases ileal) biopsy specimens were obtained by sigmoidoscopy or colonoscopy, as described previously (61). Rectosigmoid biopsy specimens were collected ~25 cm from the rectal opening using the Olympus EndoJaw disposable biopsy forceps with a channel size of 3.7 mm. Gut biopsy specimens were placed in RPMI 1640 medium (Gibco) and stored on ice until processing.

Isolation of PBMCs. PBMCs were recovered by Ficoll density gradient centrifugation from fresh venous blood as described previously (62). Whole blood was centrifuged at 1,000 $\times$ *g* at room temperature (RT) for 10 min without braking, followed by plasma removal. The remaining cells were diluted in 30 to 35 ml of phosphate-buffered saline (PBS), mixed, layered on 15 ml of Ficoll, and spun at 160 $\times$ *g* at RT for 20 min with no brake. The top 15 to 20 ml of the supernatant was aspirated to remove excess platelets, and the cells were centrifuged again at 350 $\times$ *g* at RT for 20 min without braking. The PBMC-containing layer was transferred to a fresh tube, diluted to 50 ml with PBS, spun at 400 $\times$ *g* for 8 min at RT, and washed twice more with 50 ml PBS, and cells were counted.

Isolation of total gut cells from gut biopsy specimens. Total dissociated gut cells were isolated from gut biopsy specimens using a previously described procedure (63), which incorporates 3 phases: epithelial stripping of the biopsy specimens, enzymatic degradation of the lamina propria, and mechanical dissociation. The epithelial lining was stripped, and intraepithelial cells were isolated through two rounds of 20 min of incubation in Ca^{2+}-free and Mg^{2+}-free PBS with 5 mM EDTA and 10 mM dithiothreitol (DTT) (Sigma-Aldrich) at 37°C. The supernatants from both rounds (containing intraepithelial lymphocytes) were passed through a 70-μm cell strainer, saved in a separate tube on ice, spun at 300 $\times$ *g* for 5 min, and resuspended in complete RPMI 1640 medium (Gibco). The remaining lamina propria tissue was transferred into gentleMACS C tubes (Miltenyi) and digested in 3 ml of RPMI 1640 medium containing 0.5 mg/ml of CLSPA collagenase (Worthington Biochemical Corporation) and 100 μg/ml DNase (Roche) for 30 min at 37°C under continuous rotation (40 $\times$ *g*) using an incubation shaker. After incubation, the C tubes were placed on the gentleMACS dissociator (Miltenyi), and the tissue was mechanically disrupted (program m_intestine_01). The cell suspension (containing lamina propria lymphocytes) was passed through a 70-μm cell strainer, spun at 300 $\times$ *g* for 5 min, and resuspended in fresh complete RPMI 1640 medium. Cell suspensions from the epithelium and lamina propria were combined, incubated for an additional 30 min with 100 μg/ml DNase (Roche), passed through a 40-μm cell strainer, washed, and prepared for further application.

Immunohistology. Paraformaldehyde (4%)-fixed cryosections of gut biopsy specimens were treated with 1% SDS, blocked with blocking serum (Jackson Immunoresearch), and stained with primary antibodies against CD4 (clone 4B12) and CD3 (F7.2.38) from Dako, CD8 (polyclonal) from Abcam, and CD103 (Ber-ACT8) from BD Biosciences. Secondary antibodies were anti-mouse/rabbit/goat Cy3/fluorescein isothiocyanate (FITC)/Alexa Fluor 647 (AF647) (Jackson Immunoresearch). DNA/nuclei were visualized using 4′,6-diamidino-2-phenylindole (DAPI). As negative controls, sections were stained without incubation with a primary antibody. Stained sections were observed by fluorescence microscopy (Axiovert 200 inverted microscope; Zeiss). Green, red, and blue channel images were merged with AxioVision 4.8 software. Images were enhanced for color contrast using Photoshop CS2 software (Adobe).

Cell sorting and flow cytometry. Single-cell suspensions derived from PBMCs, gut biopsy specimens, or leukapheresis were washed twice with PBS, followed by staining with the Live/Dead fixable aqua dead cell stain kit (405-nm excitation; Invitrogen) for 15 min at RT. Stained cells were washed twice with PBS, blocked for Fc receptors (human BD Fc block; BD Biosciences) for 10 min at RT, and stained with

a mixture of the following fluorochrome-conjugated anti-human primary antibodies from BD Biosciences: brilliant violet 650 (BV650) CD4 (clone SK3), BV605 CD8 (SK1), BV421 CD103 (Ber-ACT8), allophycocyanin (APC)-H7 CD45RA (HI100), AF647 CXCR5 (RF8B2), phycoerythrin (PE)-Cy7 PD-1 (EH12.1), peridinin chlorophyll protein (PerCP)-Cy5.5 CD3 (UCHT1), PE-CF594 TCR$\gamma\delta$ (B1), and FITC CD69 (FN50). Stained cells were acquired and sorted with the BD FACSAria II cell sorter utilizing FACSDiva software (BD). Acquired data were analyzed using FlowJo software (TreeStar). Cells were sorted based on the indicated sorting strategies in Fig. 3 and 5 into 5-ml round-bottom tubes containing either Tri reagent (Sigma-Aldrich) for HIV RNA and DNA quantification or FACS buffer (PBS with 15% fetal bovine serum [FBS]) for the outgrowth assay.

Characterization of surface marker expression by mass cytometry. Isolated cells were analyzed by mass cytometry (CyTOF). After single-cell suspensions of the blood- and gut-derived cells were generated, cells were stained for 1 min with 25 μM cisplatin (Sigma) in PBS as a viability marker and then quenched with CyFACS buffer (PBS with 0.1% bovine serum albumin [BSA] and 0.1% sodium azide). Cells were then fixed with 2% paraformaldehyde (PFA), washed, and then frozen until they were ready to be stained. For staining, cells were first barcoded using the Cell-ID 20-plex PD barcoding kit (Fluidigm) according to the manufacturer's instructions. Cells were then stained with antibodies against surface antigens for 45 min at 4°C and then fixed overnight in PBS supplemented with 2% PFA. Cells were permeabilized for 45 min at 4°C with permeabilization buffer (eBioscience), stained with antibodies against intracellular antigens for 30 min at 4°C, and resuspended in a 1:500 dilution of the 191/193Ir DNA intercalator (Fluidigm). A total of 38 surface and intracellular antibodies were used in the panel, 33 of which were previously validated (64). Cells were washed, resuspended in distilled water, and analyzed on a CyTOF2 instrument (Fluidigm) at the UCSF Parnassus Flow Core. EQ calibration beads (Fluidigm) were included and used for normalization across runs. Data were analyzed with FlowJo (TreeStar) and Cytobank. Events corresponding to T cells were identified based on DNA content, viability, cell length, and presence in the $CD3^+$ $CD19^-$ gate as previously described (64).

Measurement of total HIV DNA and HIV transcripts. Total cellular RNA and DNA were extracted using Tri reagent as described previously (32), including the use of polyacryl carrier (2 to 3 μl) and the optional back-extraction buffer for isolating DNA, and resuspended in a minimum of 20 μl. Levels of HIV DNA (R-U5/pre-Gag region) were measured in duplicate (8 μl of DNA/well) by ddPCR. The cell equivalents in the extracted DNA were measured by duplicate (2 μl/well) ddPCR for the human gene telomere reverse transcriptase (TERT) (2 copies/cell) and used to normalize the HIV DNA levels to 10^6 cells. Levels of total (initiated) HIV transcripts were measured in duplicate (5 μl of cDNA/well) by a polyadenylation-RT-ddPCR assay for the TAR region, except that the total RT volume was 15 μl (including 4 μl of cellular RNA). Levels of 5′-elongated (R-U5/pre-Gag region ["long-LTR"]) HIV transcripts and polyadenylated HIV transcripts {U3-poly(A) [poly(A)]} were measured in duplicate (5 μl of cDNA/well) by RT-ddPCR, except that the total RT volume was 25 μl (including 14 μl of cellular RNA). HIV RNA levels were normalized to cell numbers using the cell equivalents as determined by ddPCR for TERT (as described above), the RNA resuspension volume, and the volumes used for each RT and ddPCR well. As an alternative method of normalization to cell numbers, HIV RNA levels were also normalized to the cell counts from the sorts. The extent of HIV transcriptional elongation was also measured as the ratios of elongated to total (initiated) HIV RNAs (both expressed as copies per 10^6 cells), which are independent of any normalization to cell numbers.

Statistical analysis of cell frequencies, viral copies, and transcripts. Data analysis and visualization were performed with Prism 6.0 (GraphPad Software). Flow cytometry data were compared between HIV^+ and HIV^- participants using the Mann-Whitney U test. Comparisons between cell types in HIV DNA levels, HIV RNA levels per provirus, and HIV RNA ratios were performed in a pairwise fashion using the Wilcoxon signed-rank test. Samples with undetectable HIV DNA (rare) or RNA were assigned a value of zero. A confirmatory analysis was performed in which samples with undetectable HIV were assigned no value (blank), thus limiting the analysis to pairs in which each member had a measured value. To account for any possible error or imprecision that could be introduced by samples with very few HIV-infected cells, we also repeated the analyses using only those samples in which we measured 5 or more copies of HIV DNA. A P value of $\leq$0.05 was considered statistically significant. Correlations between HIV DNA levels and CD4 expression were performed using linear regression and Spearman correlations.

Quantification of defective and likely intact proviruses. Accelevir Diagnostics performed the IPDA generally as described previously (29), using optimized standard operating procedures developed by the company. Genomic DNA was isolated using the QIAamp DNA minikit (Qiagen). DNA concentrations were determined by fluorometry (Qubit dsDNA BR assay kit; Thermo Fisher Scientific), and DNA quality was determined by UV-visible (UV-Vis) spectrophotometry (QIAxpert; Qiagen). Genomic DNA was then analyzed by IPDAs.

Each IPDA consists of two multiplex ddPCR reactions performed in parallel: (i) the HIV-1 proviral discrimination reaction, which distinguishes intact from defective proviruses, and (ii) the copy reference/shearing reaction (Accelevir Diagnostics), which quantifies DNA shearing and input diploid cell equivalents. The HIV-1 proviral discrimination reactions employ two independent hydrolysis probe reactions that simultaneously interrogate the packaging signal (Psi) and the Rev response element (RRE) on individual proviruses to discriminate intact from defective proviruses. ddPCR droplets containing intact proviruses exhibit probe signals from both discriminatory amplicons, while droplets containing defective proviruses exhibit only one probe signal from a single discriminatory amplicon. The copy reference/shearing reactions employ two independent hydrolysis probe reactions targeting the human *RPP30* gene.

ddPCR reaction mixtures were assembled via automated liquid handlers, and ddPCR was performed on the Bio-Rad QX200 AutoDG digital droplet PCR system. An optimized thermal cycling procedure was employed (Accelevir Diagnostics). Samples were batch processed and analyzed. Operators were blind to sample identity during assay execution.

Induction of supernatant HIV RNA. Leukoreduction filters from blood donors were obtained from the Blood Systems Research Institute (BSRI) and used to isolate PBMCs, as described above. Donor CD4 T cells were isolated by negative selection using antibody-bound beads (Untouched human CD4 T$^+$ cell kit; Thermo Fisher) and activated for 1 to 2 days with PHA plus interleukin-2 (IL-2) (20 U/ml) in RPMI 1640 medium with 10% FBS, penicillin/streptomycin (10 U/ml), and L-glutamine (2 mM) ("complete RPMI" medium). Cryopreserved cells from leukapheresis (from the same 3 HIV$^+$, ART-suppressed study participants used to measure likely intact proviruses) were thawed and used to FACS sort live, singlet populations of CD3$^+$ CD8$^-$ TCR$\gamma\delta^-$ CD4$^+$ T cells into 3 populations: (i) CXCR5$^+$ PD-1^{hi} (Tfh-like), (ii) CD103$^+$, and (iii) CD103$^-$. Cells were sorted into PBS plus 15% FBS. One-fifth of each cell population was frozen for baseline HIV DNA and RNA levels, and one-fifth was activated for 2 days with anti-CD3/CD28 beads plus IL-2 (20 U/ml), indinavir, and nevirapine (no donor cells) in complete RPMI medium with 10% FBS. The remaining three-fifths of the cells were used in a modified coculture assay to assess the induction of supernatant virus, as described below.

For the induction of supernatant virus, the numbers of sorted CD103$^+$ cells from the first two participants, and of Tfh-like cells from the second participant, were deemed insufficient for replicate wells, while CD103$^-$ cells were tested in replicate. For these two participants, up to 1.2×10^6 cells from each population were activated with anti-CD3/CD28 beads plus IL-2 (20 U/ml) in complete RPMI medium with 10% FBS (at 1×10^6 cells/ml) for 90 min and then mixed with 1.2×10^6 PHA-activated donor CD4 T cells from each of 2 donors in complete RPMI medium with 10% FBS plus IL-2 (1×10^6 cells/ml) in 6-well plates. After 2 days, when cells began to proliferate and the culture medium started to turn color, partial exchanges of the medium (same volume [up to half of the total] from each well) were performed as needed to prevent the medium from turning orange. Prior to day 7, residual cells in the aspirated medium were pelleted at $300 \times g$ for 6 min, resuspended in fresh medium, and returned to the well. At day 7, half of the medium was removed, cells were pelleted and frozen at −80°C, and each well was supplemented with 1×10^6 freshly PHA-activated donor CD4 T cells from each of two donors. After day 7, medium exchanges were performed as needed, but cells were not returned to the wells. Cultures were terminated at day 16 (first participant) and day 10 (second participant).

For the third study participant, in whom yields of each cell type were higher, we adopted a different method designed to test each cell type with replicate, terminal dilutions containing the same number of cells and to maximize opportunities for allogeneic stimulation and spreading infection by "crowding" the patient cells with a higher ratio of donor cells in a smaller volume. On the day of sorting, replicates of 10^4 cells of each cell type were seeded in 96-well V-bottom plates with anti-CD3/CD28 beads and IL-2 (20 U/ml) in complete RPMI medium with 10% FBS. The next morning, each well was supplemented with PHA-activated donor CD4 T cells (10^5 cells from each of 2 donors, each in 100 μl of complete RPMI medium with FBS plus IL-2). On day 4, when cells had started to divide, pairs of 2 wells from each cell type were combined into the larger wells of 48-well plates and supplemented with fresh medium. Fresh medium was also added on days 5 and 6. On day 7, sets of 12 wells of each cell type from the 48-well plates (corresponding to 2.4×10^5 cells of the original patient cells) were combined, and cells and the supernatant were saved.

Cell-free supernatants were obtained at various time points by pelleting residual cells at $300 \times g$ for 6 min, aspirating the supernatant, centrifuging the supernatant again at $1{,}000 \times g$ for 6 min to remove any remaining cells or debris, aspirating the supernatant, and freezing the supernatant at −80°C. Cell-free supernatants (0.7 to 1.0 ml) were thawed and tested for HIV RNA using the Abbott RealTime HIV platform, as performed by the clinical laboratory, using the same process used to measure viral loads in the plasma of HIV-infected participants. For the third study participant, where replicates were available for each cell type, we calculated the frequency of each cell type that could be induced to produce supernatant HIV RNA using the total number of replicates and the number of replicates with detectable supernatant HIV RNA at day 7 according to the method of extreme-limiting-dilution analysis (ELDA) (65).

RNA sequencing and library preparation. RNA was isolated using a column-based method (Qiagen RNeasy kit), and quality control (QC) was performed on the Agilent 2100 bioanalyzer. Strand-specific RNA-seq libraries were prepared using the Ovation SoLo RNA-seq solution (NuGEN, a Tecan Group company), according to the manufacturer's instructions. The total RNA was DNase treated, and cDNA was generated with random and poly(T) primers. Following library construction, unwanted rRNA transcripts were removed using NuGEN's AnyDeplete technology (formerly InDA-C) using the human rRNA probe mix. RNA-seq libraries were analyzed with the Agilent 2100 bioanalyzer and quantified by quantitative PCR (qPCR) specific for Illumina libraries (Kapa library quantification kit; Roche Sequencing). High-throughput sequencing was performed using a NextSeq 500 instrument (Illumina), replacing the Illumina read 1 primer with the NuGEN Ovation SoLo custom R1 primer. Sixteen base pairs of index I, containing an 8-bp barcode followed by an 8-bp randomer, were sequenced to allow the identification of unique molecules.

RNA-seq quality control. RNA-seq QC checks were performed using FastQC (http://www.bioinformatics.babraham.ac.uk/projects/fastqc) and RseQC (66). Adapter and read quality trimming were performed with fastq-mcf (Quintiles Company). Reads were mapped to the hg19 genome assembly using STAR (67). Ambiguously mapping reads were discarded. Read duplicates were removed using NuGEN's NuDup software, which relies on unique molecular identifiers (UMIs). Following UMI-based deduplication, the raw gene count matrix was obtained using Subread's featureCounts (68). Read mapping and QC statistics

were summarized and visualized with MultiQC (69). One outlier with low RNA quality was identified in the QC and evident in principal-component (PC) plots. A new patient was recruited to replace the patient with an outlier sample. QC measures and PC plots showed the replacement to be of good quality and confirmed that the outlier sample was anomalous.

Differential gene expression. edgeR was used for normalization and differential gene expression tests. Normalization factors were calculated using the default method (trimmed mean of M values [TMM]) with default parameters (70). A single joint model without an intercept was fit in edgeR to facilitate testing specific hypotheses while leveraging information across all replicates and conditions for estimating dispersion. A single group factor was used in the model, which comprised all possible combinations of the three experimental variables (i.e., HIV status, tissue, and CD103 type). Hypothesis tests were performed in edgeR using the gmlLRT function (71). Heat maps were generated using heatmaply (72). Volcano and PC plots were generated using ggplot2 (73). The following cutoffs were used for the volcano plots: a $\log_2$ expression fold change of >1 and a false discovery rate (FDR)-adjusted P value of <0.05. Venn diagrams were generated using Vennerable (J. Swinton [https://github.com/js229/Vennerable]).

Pathway analysis: functional enrichment. The gene set resulting from the Venn intersection differential expression analysis consisted of 376 genes significantly upregulated in x (FDR.x of <0.05 and log fold change of x [logFC.x] of >0) and downregulated in y (FDR.y of <0.05 and logFC.y of <0) and 354 genes with the opposite regulation pattern. The recognized gene symbols for these two sets were submitted to the Enrichr tool for functional enrichment analysis (74). Enrichment results from Gene Ontology biological processes and WikiPathways were exported (75). A combined score was calculated for representative terms of interest from the statistics provided by Enrichr, $-\log$ (adjusted P value) $\times$ Z-score, and bar plots were generated using the ggpubr R package.

CORUM analysis: detection of complexes. The gene set resulting from the pairwise differential expression analysis between $CD103^+$ and $CD103^-$ blood cells consisted of 875 significantly regulated genes (FDR < 0.05). The 875 Ensembl identifiers were translated to UniProt identifiers using the biomaRt package and used to subset a custom version of the CORUM database of protein complexes (76) (courtesy of David Jimenez-Morales). The annotated binary interactions that overlapped our gene set were loaded into Cytoscape using the RCy3 Bioconductor package (77). Subnetworks of selected complexes were extracted based on edge annotations from CORUM using Cytoscape.

STRING analysis: network reconstruction of ontology terms. The genes annotated by the following ontology terms from Gene Ontology biological processes and VirusMINT (78) were collected into a single set and used to query the STRING database for network reconstruction: steroid regulatory element binding protein (SREBP) signaling pathway (GO:0032933), positive regulation of intrinsic apoptotic signaling pathway by p53 class mediator (GO:1902255), late viral transcription (GO:0019086), Epstein-Barr virus (strain GD1), and human immunodeficiency virus type 1. The query was performed using the STRING app for Cytoscape with a default edge score threshold of 0.4 and allowing for no additional nodes (79). The 140-gene query resulted in a network of 98 genes connected by 2,077 interactions. Approximately 2,000 of these interactions were shared among 63 ribosomal proteins involved in common protein complexes. This complex was collapsed into a group node (or metanode), which maintains the calculated mean of any attribute values associated with its member nodes, e.g., logFC.

Network and pathway visualization. Networks and complexes were loaded into Cytoscape as described above. Pathways of interest, e.g., those identified by functional enrichment analysis, were loaded from WikiPathways (75) into Cytoscape using the WikiPathways app (80). Differential expression results were loaded into Cytoscape using the built-in table importer and then mapped to node fill color using Cytoscape's visual style features.

SUPPLEMENTAL MATERIAL

Supplemental material is available online only.

SUPPLEMENTAL FILE 1, PDF file, 1.4 MB.
SUPPLEMENTAL FILE 2, XLSX file, 1.9 MB.
SUPPLEMENTAL FILE 3, XLSX file, 1.9 MB.
SUPPLEMENTAL FILE 4, XLSX file, 1.9 MB.
SUPPLEMENTAL FILE 5, XLSX file, 1.9 MB.
SUPPLEMENTAL FILE 6, XLSX file, 2 MB.
SUPPLEMENTAL FILE 7, XLSX file, 1.9 MB.
SUPPLEMENTAL FILE 8, XLSX file, 2 MB.
SUPPLEMENTAL FILE 9, XLSX file, 2 MB.

ACKNOWLEDGMENTS

We thank the SCOPE study coordinators, Montha Pao and Rebecca Hoh, and the study participants.

This work was supported as part of the amfAR Institute for HIV Cure Research (amfAR grant number 109301). S.S. was also supported by the National Institutes of Health (NIH) (DP2 AI112244) and a California HIV/AIDS Research Program IDEA award (CHRP ID15-GI-059). S.A.Y. was supported by the National Institutes of Health (R01DK108349,

R01AI132128, and R01DK120387). S.K. was supported by a University of California, San Francisco, Gladstone Institute of Virology and Immunology Center for AIDS Research (CFAR) mentored scientist award (P30 AI027763). N.R.R. and G.X. were supported by the NIH (R01 AI127219, R01 AI147777, and P01 AI131374). Accelevir Diagnostics acknowledges support by SBIR grants from the NIH (R44AI124996) and NSF (1738428). This publication was made possible with help from CFAR, an NIH-funded program (P30 AI027763), NIH S10 RR028962, and the James B. Pendleton Charitable Trust, all supporting the Gladstone Flow Core and cell sorter. The funders had no role in study design, data collection and interpretation, or the decision to submit the work for publication.

Conceptualization, S.S., S.A.Y., S.K., and P.W.H.; Methodology, S.K., T.-H.C., M.T., F.W., S.S., S.A.Y., G.X., S.T., D.F., A.R.P., G.M.L., K.D.R., N.R.R., N.G.J., J.M.M., C.M.L., R.F.S., and M.S.; Formal Analysis, S.S., S.K., S.A.Y., N.R.R., M.T., and A.R.P.; Resources, S.S., S.A.Y., R.F.S., N.R.R., S.G.D., C.M.L., M.S., and P.W.H.; Writing – Original Draft, S.S., S.A.Y., S.K., and M.T.; Writing – Review & Editing, S.A.Y., S.S., S.K., T.-H.C., M.T., F.W., D.F., A.R.P., G.M.L., N.G.J., N.R.R., S.T., P.W.H., R.F.S., K.D.R., C.M.L., J.M.M., M.S., and S.G.D.; Visualization, S.S., S.K., S.A.Y., M.T., S.T., and A.R.P.; Supervision, S.S., S.A.Y., G.M.L., N.R.R., and J.M.M.; Funding Acquisition, S.S., S.A.Y., S.K., G.M.L., P.W.H., and N.R.R.

Aspects of the IPDA are the subject of a patent application, PCT/US16/28822, filed by Johns Hopkins University. R.F.S. is an inventor on this patent application. Accelevir Diagnostics holds an exclusive license for this patent application. G.M.L. and K.D.R. are employees of Accelevir Diagnostics, and G.M.L. is a shareholder in Accelevir Diagnostics. R.F.S. holds no equity interest in Accelevir Diagnostics.

REFERENCES

1. Chun TW, Carruth L, Finzi D, Shen X, DiGiuseppe JA, Taylor H, Hermankova M, Chadwick K, Margolick J, Quinn TC, Kuo YH, Brookmeyer R, Zeiger MA, Barditch-Crovo P, Siliciano RF. 1997. Quantification of latent tissue reservoirs and total body viral load in HIV-1 infection. Nature 387:183–188. https://doi.org/10.1038/387183a0.
2. Finzi D, Hermankova M, Pierson T, Carruth LM, Buck C, Chaisson RE, Quinn TC, Chadwick K, Margolick J, Brookmeyer R, Gallant J, Markowitz M, Ho DD, Richman DD, Siliciano RF. 1997. Identification of a reservoir for HIV-1 in patients on highly active antiretroviral therapy. Science 278:1295–1300. https://doi.org/10.1126/science.278.5341.1295.
3. Wong JK, Hezareh M, Gunthard HF, Havlir DV, Ignacio CC, Spina CA, Richman DD. 1997. Recovery of replication-competent HIV despite prolonged suppression of plasma viremia. Science 278:1291–1295. https://doi.org/10.1126/science.278.5341.1291.
4. Khan S, Telwatte S, Trapecar M, Yukl S, Sanjabi S. 2017. Differentiating immune cell targets in gut-associated lymphoid tissue for HIV cure. AIDS Res Hum Retroviruses 33:S40–S58. https://doi.org/10.1089/AID.2017.0153.
5. Poles MA, Boscardin WJ, Elliott J, Taing P, Fuerst MM, McGowan I, Brown S, Anton PA. 2006. Lack of decay of HIV-1 in gut-associated lymphoid tissue reservoirs in maximally suppressed individuals. J Acquir Immune Defic Syndr 43:65–68. https://doi.org/10.1097/01.qai.0000230524.71717.14.
6. Belmonte L, Olmos M, Fanin A, Parodi C, Bare P, Concetti H, Perez H, de Bracco MM, Cahn P. 2007. The intestinal mucosa as a reservoir of HIV-1 infection after successful HAART. AIDS 21:2106–2108. https://doi.org/10.1097/QAD.0b013e3282efb74b.
7. Chun TW, Nickle DC, Justement JS, Meyers JH, Roby G, Hallahan CW, Kottilil S, Moir S, Mican JM, Mullins JI, Ward DJ, Kovacs JA, Mannon PJ, Fauci AS. 2008. Persistence of HIV in gut-associated lymphoid tissue despite long-term antiretroviral therapy. J Infect Dis 197:714–720. https://doi.org/10.1086/527324.
8. Yukl SA, Gianella S, Sinclair E, Epling L, Li Q, Duan L, Choi AL, Girling V, Ho T, Li P, Fujimoto K, Lampiris H, Hare CB, Pandori M, Haase AT, Gunthard HF, Fischer M, Shergill AK, McQuaid K, Havlir DV, Wong JK. 2010. Differences in HIV burden and immune activation within the gut of HIV-positive patients receiving suppressive antiretroviral therapy. J Infect Dis 202:1553–1561. https://doi.org/10.1086/656722.
9. d'Ettorre G, Paiardini M, Zaffiri L, Andreotti M, Ceccarelli G, Rizza C, Indinnimeo M, Vella S, Mastroianni CM, Silvestri G, Vullo V. 2011. HIV persistence in the gut mucosa of HIV-infected subjects undergoing antiretroviral therapy correlates with immune activation and increased levels of LPS. Curr HIV Res 9:148–153. https://doi.org/10.2174/157016211795945296.
10. Eriksson S, Graf EH, Dahl V, Strain MC, Yukl SA, Lysenko ES, Bosch RJ, Lai J, Chioma S, Emad F, Abdel-Mohsen M, Hoh R, Hecht F, Hunt P, Somsouk M, Wong J, Johnston R, Siliciano RF, Richman DD, O'Doherty U, Palmer S, Deeks SG, Siliciano JD. 2013. Comparative analysis of measures of viral reservoirs in HIV-1 eradication studies. PLoS Pathog 9:e1003174. https://doi.org/10.1371/journal.ppat.1003174.
11. Yukl SA, Shergill AK, Ho T, Killian M, Girling V, Epling L, Li P, Wong LK, Crouch P, Deeks SG, Havlir DV, McQuaid K, Sinclair E, Wong JK. 2013. The distribution of HIV DNA and RNA in cell subsets differs in gut and blood of HIV-positive patients on ART: implications for viral persistence. J Infect Dis 208:1212–1220. https://doi.org/10.1093/infdis/jit308.
12. Estes JD, Kityo C, Ssali F, Swainson L, Makamdop KN, Del Prete GQ, Deeks SG, Luciw PA, Chipman JG, Beilman GJ, Hoskuldsson T, Khoruts A, Anderson J, Deleage C, Jasurda J, Schmidt TE, Hafertepe M, Callisto SP, Pearson H, Reimann T, Schuster J, Schoephoerster J, Southern P, Perkey K, Shang L, Wietgrefe SW, Fletcher CV, Lifson JD, Douek DC, McCune JM, Haase AT, Schacker TW. 2017. Defining total-body AIDS-virus burden with implications for curative strategies. Nat Med 23:1271–1276. https://doi.org/10.1038/nm.4411.
13. Vandergeeten C, Fromentin R, Chomont N. 2012. The role of cytokines in the establishment, persistence and eradication of the HIV reservoir. Cytokine Growth Factor Rev 23:143–149. https://doi.org/10.1016/j.cytogfr.2012.05.001.
14. Besnard E, Hakre S, Kampmann M, Lim HW, Hosmane NN, Martin A, Bassik MC, Verschueren E, Battivelli E, Chan J, Svensson JP, Gramatica A, Conrad RJ, Ott M, Greene WC, Krogan NJ, Siliciano RF, Weissman JS, Verdin E. 2016. The mTOR complex controls HIV latency. Cell Host Microbe 20:785–797. https://doi.org/10.1016/j.chom.2016.11.001.
15. Kulpa DA, Talla A, Brehm JH, Ribeiro SP, Yuan S, Bebin-Blackwell AG, Miller M, Barnard R, Deeks SG, Hazuda D, Chomont N, Sekaly RP. 2019. Differentiation into an effector memory phenotype potentiates HIV-1 latency reversal in CD4+ T cells. J Virol 93:e00969-19. https://doi.org/10.1128/JVI.00969-19.
16. Dobrowolski C, Valadkhan S, Graham AC, Shukla M, Ciuffi A, Telenti A,

Karn J. 2019. Entry of polarized effector cells into quiescence forces HIV latency. mBio 10:e00337-19. https://doi.org/10.1128/mBio.00337-19.
17. Cepek KL, Shaw SK, Parker CM, Russell GJ, Morrow JS, Rimm DL, Brenner MB. 1994. Adhesion between epithelial cells and T lymphocytes mediated by E-cadherin and the alpha E beta 7 integrin. Nature 372:190–193. https://doi.org/10.1038/372190a0.
18. El-Asady R, Yuan R, Liu K, Wang D, Gress RE, Lucas PJ, Drachenberg CB, Hadley GA. 2005. TGF-beta-dependent CD103 expression by CD8(+) T cells promotes selective destruction of the host intestinal epithelium during graft-versus-host disease. J Exp Med 201:1647–1657. https://doi.org/10.1084/jem.20041044.
19. Thome JJ, Farber DL. 2015. Emerging concepts in tissue-resident T cells: lessons from humans. Trends Immunol 36:428–435. https://doi.org/10.1016/j.it.2015.05.003.
20. Klicznik MM, Morawski PA, Hollbacher B, Varkhande SR, Motley SJ, Kuri-Cervantes L, Goodwin E, Rosenblum MD, Long SA, Brachtl G, Duhen T, Betts MR, Campbell DJ, Gratz IK. 2019. Human CD4$^+$ CD103$^+$ cutaneous resident memory T cells are found in the circulation of healthy individuals. Sci Immunol 4:eaav8995. https://doi.org/10.1126/sciimmunol.aav8995.
21. Evans VA, van der Sluis RM, Solomon A, Dantanarayana A, McNeil C, Garsia R, Palmer S, Fromentin R, Chomont N, Sekaly RP, Cameron PU, Lewin SR. 2018. Programmed cell death-1 contributes to the establishment and maintenance of HIV-1 latency. AIDS 32:1491–1497. https://doi.org/10.1097/QAD.0000000000001849.
22. Fromentin R, Bakeman W, Lawani MB, Khoury G, Hartogensis W, DaFonseca S, Killian M, Epling L, Hoh R, Sinclair E, Hecht FM, Bacchetti P, Deeks SG, Lewin SR, Sekaly RP, Chomont N. 2016. CD4$^+$ T cells expressing PD-1, TIGIT and LAG-3 contribute to HIV persistence during ART. PLoS Pathog 12:e1005761. https://doi.org/10.1371/journal.ppat.1005761.
23. Fromentin R, DaFonseca S, Costiniuk CT, El-Far M, Procopio FA, Hecht FM, Hoh R, Deeks SG, Hazuda DJ, Lewin SR, Routy JP, Sekaly RP, Chomont N. 2019. PD-1 blockade potentiates HIV latency reversal ex vivo in CD4(+) T cells from ART-suppressed individuals. Nat Commun 10:814. https://doi.org/10.1038/s41467-019-08798-7.
24. Xu Y, Weatherall C, Bailey M, Alcantara S, De Rose R, Estaquier J, Wilson K, Suzuki K, Corbeil J, Cooper DA, Kent SJ, Kelleher AD, Zaunders J. 2013. Simian immunodeficiency virus infects follicular helper CD4 T cells in lymphoid tissues during pathogenic infection of pigtail macaques. J Virol 87:3760–3773. https://doi.org/10.1128/JVI.02497-12.
25. Perreau M, Savoye AL, De Crignis E, Corpataux JM, Cubas R, Haddad EK, De Leval L, Graziosi C, Pantaleo G. 2013. Follicular helper T cells serve as the major CD4 T cell compartment for HIV-1 infection, replication, and production. J Exp Med 210:143–156. https://doi.org/10.1084/jem.20121932.
26. Banga R, Procopio FA, Noto A, Pollakis G, Cavassini M, Ohmiti K, Corpataux JM, de Leval L, Pantaleo G, Perreau M. 2016. PD-1(+) and follicular helper T cells are responsible for persistent HIV-1 transcription in treated aviremic individuals. Nat Med 22:754–761. https://doi.org/10.1038/nm.4113.
27. Bruner KM, Murray AJ, Pollack RA, Soliman MG, Laskey SB, Capoferri AA, Lai J, Strain MC, Lada SM, Hoh R, Ho YC, Richman DD, Deeks SG, Siliciano JD, Siliciano RF. 2016. Defective proviruses rapidly accumulate during acute HIV-1 infection. Nat Med 22:1043–1049. https://doi.org/10.1038/nm.4156.
28. Ho YC, Shan L, Hosmane NN, Wang J, Laskey SB, Rosenbloom DI, Lai J, Blankson JN, Siliciano JD, Siliciano RF. 2013. Replication-competent noninduced proviruses in the latent reservoir increase barrier to HIV-1 cure. Cell 155:540–551. https://doi.org/10.1016/j.cell.2013.09.020.
29. Bruner KM, Wang Z, Simonetti FR, Bender AM, Kwon KJ, Sengupta S, Fray EJ, Beg SA, Antar AAR, Jenike KM, Bertagnolli LN, Capoferri AA, Kufera JT, Timmons A, Nobles C, Gregg J, Wada N, Ho YC, Zhang H, Margolick JB, Blankson JN, Deeks SG, Bushman FD, Siliciano JD, Laird GM, Siliciano RF. 2019. A quantitative approach for measuring the reservoir of latent HIV-1 proviruses. Nature 566:120–125. https://doi.org/10.1038/s41586-019-0898-8.
30. Lundquist CA, Tobiume M, Zhou J, Unutmaz D, Aiken C. 2002. Nef-mediated downregulation of CD4 enhances human immunodeficiency virus type 1 replication in primary T lymphocytes. J Virol 76:4625–4633. https://doi.org/10.1128/jvi.76.9.4625-4633.2002.
31. Telwatte S, Lee S, Somsouk M, Hatano H, Baker C, Kaiser P, Kim P, Chen TH, Milush J, Hunt PW, Deeks SG, Wong JK, Yukl SA. 2018. Gut and blood differ in constitutive blocks to HIV transcription, suggesting tissue-specific differences in the mechanisms that govern HIV latency. PLoS Pathog 14:e1007357. https://doi.org/10.1371/journal.ppat.1007357.
32. Yukl SA, Kaiser P, Kim P, Telwatte S, Joshi SK, Vu M, Lampiris H, Wong JK. 2018. HIV latency in isolated patient CD4$^+$ T cells may be due to blocks in HIV transcriptional elongation, completion, and splicing. Sci Transl Med 10:eaap9927. https://doi.org/10.1126/scitranslmed.aap9927.
33. Soriano-Sarabia N, Archin NM, Bateson R, Dahl NP, Crooks AM, Kuruc JD, Garrido C, Margolis DM. 2015. Peripheral Vgamma9Vdelta2 T cells are a novel reservoir of latent HIV infection. PLoS Pathog 11:e1005201. https://doi.org/10.1371/journal.ppat.1005201.
34. Gatignol A, Buckler-White A, Berkhout B, Jeang KT. 1991. Characterization of a human TAR RNA-binding protein that activates the HIV-1 LTR. Science 251:1597–1600. https://doi.org/10.1126/science.2011739.
35. Sanghvi VR, Steel LF. 2011. The cellular TAR RNA binding protein, TRBP, promotes HIV-1 replication primarily by inhibiting the activation of double-stranded RNA-dependent kinase PKR. J Virol 85:12614–12621. https://doi.org/10.1128/JVI.05240-11.
36. Dorin D, Bonnet MC, Bannwarth S, Gatignol A, Meurs EF, Vaquero C. 2003. The TAR RNA-binding protein, TRBP, stimulates the expression of TAR-containing RNAs in vitro and in vivo independently of its ability to inhibit the dsRNA-dependent kinase PKR. J Biol Chem 278:4440–4448. https://doi.org/10.1074/jbc.M208954200.
37. Tan H, Yang K, Li Y, Shaw TI, Wang Y, Blanco DB, Wang X, Cho JH, Wang H, Rankin S, Guy C, Peng J, Chi H. 2017. Integrative proteomics and phosphoproteomics profiling reveals dynamic signaling networks and bioenergetics pathways underlying T cell activation. Immunity 46:488–503. https://doi.org/10.1016/j.immuni.2017.02.010.
38. Chapman NM, Boothby MR, Chi H. 2020. Metabolic coordination of T cell quiescence and activation. Nat Rev Immunol 20:55–70. https://doi.org/10.1038/s41577-019-0203-y.
39. Wolf T, Jin W, Zoppi G, Vogel IA, Akhmedov M, Bleck CKE, Beltraminelli T, Rieckmann JC, Ramirez NJ, Benevento M, Notarbartolo S, Bumann D, Meissner F, Grimbacher B, Mann M, Lanzavecchia A, Sallusto F, Kwee I, Geiger R. 2020. Dynamics in protein translation sustaining T cell preparedness. Nat Immunol 21:927–937. https://doi.org/10.1038/s41590-020-0714-5.
40. Miyara M, Gorochov G, Ehrenstein M, Musset L, Sakaguchi S, Amoura Z. 2011. Human FoxP3$^+$ regulatory T cells in systemic autoimmune diseases. Autoimmun Rev 10:744–755. https://doi.org/10.1016/j.autrev.2011.05.004.
41. Zhou L, Lopes JE, Chong MM, Ivanov II, Min R, Victora GD, Shen Y, Du J, Rubtsov YP, Rudensky AY, Ziegler SF, Littman DR. 2008. TGF-beta-induced Foxp3 inhibits T(H)17 cell differentiation by antagonizing RORgammat function. Nature 453:236–240. https://doi.org/10.1038/nature06878.
42. Monteiro P, Gosselin A, Wacleche VS, El-Far M, Said EA, Kared H, Grandvaux N, Boulassel MR, Routy JP, Ancuta P. 2011. Memory CCR6+CD4+ T cells are preferential targets for productive HIV type 1 infection regardless of their expression of integrin beta7. J Immunol 186:4618–4630. https://doi.org/10.4049/jimmunol.1004151.
43. Khoury G, Anderson JL, Fromentin R, Hartogenesis W, Smith MZ, Bacchetti P, Hecht FM, Chomont N, Cameron PU, Deeks SG, Lewin SR. 2016. Persistence of integrated HIV DNA in CXCR3+ CCR6+ memory CD4+ T cells in HIV-infected individuals on antiretroviral therapy. AIDS 30:1511–1520. https://doi.org/10.1097/QAD.0000000000001029.
44. Gosselin A, Wiche Salinas TR, Planas D, Wacleche VS, Zhang Y, Fromentin R, Chomont N, Cohen EA, Shacklett B, Mehraj V, Ghali MP, Routy JP, Ancuta P. 2017. HIV persists in CCR6+CD4+ T cells from colon and blood during antiretroviral therapy. AIDS 31:35–48. https://doi.org/10.1097/QAD.0000000000001309.
45. Anderson JL, Khoury G, Fromentin R, Solomon A, Chomont N, Sinclair E, Milush JM, Hartogensis W, Bacchetti P, Roche M, Tumpach C, Gartner M, Pitman MC, Epling CL, Hoh R, Hecht FM, Somsouk M, Cameron PU, Deeks SG, Lewin SR. 2020. Human immunodeficiency virus (HIV)-infected CCR6+ rectal CD4+ T cells and HIV persistence on antiretroviral therapy. J Infect Dis 221:744–755. https://doi.org/10.1093/infdis/jiz509.
46. Miyara M, Sakaguchi S. 2011. Human FoxP3(+)CD4(+) regulatory T cells: their knowns and unknowns. Immunol Cell Biol 89:346–351. https://doi.org/10.1038/icb.2010.137.
47. Cantero-Perez J, Grau-Exposito J, Serra-Peinado C, Rosero DA, Luque-Ballesteros L, Astorga-Gamaza A, Castellvi J, Sanhueza T, Tapia G, Lloveras B, Fernandez MA, Prado JG, Sole-Sedeno JM, Tarrats A, Lecumberri C, Manalich-Barrachina L, Centeno-Mediavilla C, Falco V, Buzon MJ, Genesca M. 2019. Resident memory T cells are a cellular reservoir for HIV in the cervical mucosa. Nat Commun 10:4739. https://doi.org/10.1038/s41467-019-12732-2.

48. Brenchley JM, Price DA, Schacker TW, Asher TE, Silvestri G, Rao S, Kazzaz Z, Bornstein E, Lambotte O, Altmann D, Blazar BR, Rodriguez B, Teixeira-Johnson L, Landay A, Martin JN, Hecht FM, Picker LJ, Lederman MM, Deeks SG, Douek DC. 2006. Microbial translocation is a cause of systemic immune activation in chronic HIV infection. Nat Med 12:1365–1371. https://doi.org/10.1038/nm1511.
49. Yukl SA, Shergill AK, Girling V, Li Q, Killian M, Epling L, Li P, Kaiser P, Haase A, Havlir DV, McQuaid K, Sinclair E, Wong JK. 2015. Site-specific differences in T cell frequencies and phenotypes in the blood and gut of HIV-uninfected and ART-treated HIV$^+$ adults. PLoS One 10:e0121290. https://doi.org/10.1371/journal.pone.0121290.
50. Rogler G, Hausmann M, Vogl D, Aschenbrenner E, Andus T, Falk W, Andreesen R, Scholmerich J, Gross V. 1998. Isolation and phenotypic characterization of colonic macrophages. Clin Exp Immunol 112:205–215. https://doi.org/10.1046/j.1365-2249.1998.00557.x.
51. Karn J, Stoltzfus CM. 2012. Transcriptional and posttranscriptional regulation of HIV-1 gene expression. Cold Spring Harb Perspect Med 2:a006916. https://doi.org/10.1101/cshperspect.a006916.
52. Chang CC, Naranbhai V, Stern J, Roche M, Dantanarayana A, Ke R, Tennakoon S, Solomon A, Hoh R, Hartogensis W, Hecht FM, Sikaris K, Price DJ, Elliott JH, Deeks SG, Churchill M, Cameron PU, Hengartner N, Perelson AS, Lewin SR. 2018. Variation in cell-associated unspliced HIV RNA on antiretroviral therapy is associated with the circadian regulator brain-and-muscle-ARNT-like-1. AIDS 32:2119–2128. https://doi.org/10.1097/QAD.0000000000001937.
53. Revollo JR, Li X. 2013. The ways and means that fine tune Sirt1 activity. Trends Biochem Sci 38:160–167. https://doi.org/10.1016/j.tibs.2012.12.004.
54. Yeung F, Hoberg JE, Ramsey CS, Keller MD, Jones DR, Frye RA, Mayo MW. 2004. Modulation of NF-kappaB-dependent transcription and cell survival by the SIRT1 deacetylase. EMBO J 23:2369–2380. https://doi.org/10.1038/sj.emboj.7600244.
55. Pinzone MR, Cacopardo B, Condorelli F, Di Rosa M, Nunnari G. 2013. Sirtuin-1 and HIV-1: an overview. Curr Drug Targets 14:648–652. https://doi.org/10.2174/1389450111314060005.
56. Chen XY, Zhang HS, Wu TC, Sang WW, Ruan Z. 2013. Down-regulation of NAMPT expression by miR-182 is involved in Tat-induced HIV-1 long terminal repeat (LTR) transactivation. Int J Biochem Cell Biol 45:292–298. https://doi.org/10.1016/j.biocel.2012.11.002.
57. Sun WW, Jiao S, Sun L, Zhou Z, Jin X, Wang JH. 2018. SUN2 modulates HIV-1 infection and latency through association with lamin A/C to maintain the repressive chromatin. mBio 9:e02408-17. https://doi.org/10.1128/mBio.02408-17.
58. Chen J, Lopez-Moyado IF, Seo H, Lio CJ, Hempleman LJ, Sekiya T, Yoshimura A, Scott-Browne JP, Rao A. 2019. NR4A transcription factors limit CAR T cell function in solid tumours. Nature 567:530–534. https://doi.org/10.1038/s41586-019-0985-x.
59. Liu X, Wang Y, Lu H, Li J, Yan X, Xiao M, Hao J, Alekseev A, Khong H, Chen T, Huang R, Wu J, Zhao Q, Wu Q, Xu S, Wang X, Jin W, Yu S, Wang Y, Wei L, Wang A, Zhong B, Ni L, Liu X, Nurieva R, Ye L, Tian Q, Bian XW, Dong C. 2019. Genome-wide analysis identifies NR4A1 as a key mediator of T cell dysfunction. Nature 567:525–529. https://doi.org/10.1038/s41586-019-0979-8.
60. Duverger A, Wolschendorf F, Zhang M, Wagner F, Hatcher B, Jones J, Cron RQ, van der Sluis RM, Jeeninga RE, Berkhout B, Kutsch O. 2013. An AP-1 binding site in the enhancer/core element of the HIV-1 promoter controls the ability of HIV-1 to establish latent infection. J Virol 87:2264–2277. https://doi.org/10.1128/JVI.01594-12.
61. Somsouk M, Estes JD, Deleage C, Dunham RM, Albright R, Inadomi JM, Martin JN, Deeks SG, McCune JM, Hunt PW. 2015. Gut epithelial barrier and systemic inflammation during chronic HIV infection. AIDS 29:43–51. https://doi.org/10.1097/QAD.0000000000000511.
62. Yukl SA, Shergill AK, McQuaid K, Gianella S, Lampiris H, Hare CB, Pandori M, Sinclair E, Gunthard HF, Fischer M, Wong JK, Havlir DV. 2010. Effect of raltegravir-containing intensification on HIV burden and T-cell activation in multiple gut sites of HIV-positive adults on suppressive antiretroviral therapy. AIDS 24:2451–2460. https://doi.org/10.1097/QAD.0b013e32833ef7bb.
63. Trapecar M, Khan S, Roan NR, Chen TH, Telwatte S, Deswal M, Pao M, Somsouk M, Deeks SG, Hunt PW, Yukl S, Sanjabi S. 2017. An optimized and validated method for isolation and characterization of lymphocytes from HIV$^+$ human gut biopsies. AIDS Res Hum Retroviruses 33:S31–S39. https://doi.org/10.1089/AID.2017.0208.
64. Cavrois M, Banerjee T, Mukherjee G, Raman N, Hussien R, Rodriguez BA, Vasquez J, Spitzer MH, Lazarus NH, Jones JJ, Ochsenbauer C, McCune JM, Butcher EC, Arvin AM, Sen N, Greene WC, Roan NR. 2017. Mass cytometric analysis of HIV entry, replication, and remodeling in tissue CD4$^+$ T cells. Cell Rep 20:984–998. https://doi.org/10.1016/j.celrep.2017.06.087.
65. Hu Y, Smyth GK. 2009. ELDA: extreme limiting dilution analysis for comparing depleted and enriched populations in stem cell and other assays. J Immunol Methods 347:70–78. https://doi.org/10.1016/j.jim.2009.06.008.
66. Wang L, Wang S, Li W. 2012. RSeQC: quality control of RNA-seq experiments. Bioinformatics 28:2184–2185. https://doi.org/10.1093/bioinformatics/bts356.
67. Dobin A, Davis CA, Schlesinger F, Drenkow J, Zaleski C, Jha S, Batut P, Chaisson M, Gingeras TR. 2013. STAR: ultrafast universal RNA-seq aligner. Bioinformatics 29:15–21. https://doi.org/10.1093/bioinformatics/bts635.
68. Liao Y, Smyth GK, Shi W. 2014. featureCounts: an efficient general purpose program for assigning sequence reads to genomic features. Bioinformatics 30:923–930. https://doi.org/10.1093/bioinformatics/btt656.
69. Ewels P, Magnusson M, Lundin S, Kaller M. 2016. MultiQC: summarize analysis results for multiple tools and samples in a single report. Bioinformatics 32:3047–3048. https://doi.org/10.1093/bioinformatics/btw354.
70. Robinson MD, Oshlack A. 2010. A scaling normalization method for differential expression analysis of RNA-seq data. Genome Biol 11:R25. https://doi.org/10.1186/gb-2010-11-3-r25.
71. McCarthy DJ, Chen Y, Smyth GK. 2012. Differential expression analysis of multifactor RNA-Seq experiments with respect to biological variation. Nucleic Acids Res 40:4288–4297. https://doi.org/10.1093/nar/gks042.
72. Galili T, O'Callaghan A, Sidi J, Sievert C. 2018. heatmaply: an R package for creating interactive cluster heatmaps for online publishing. Bioinformatics 34:1600–1602. https://doi.org/10.1093/bioinformatics/btx657.
73. Wickham H. 2009. ggplot2: elegant graphics for data analysis. Springer Publishing Company, Inc, New York, NY.
74. Kuleshov MV, Jones MR, Rouillard AD, Fernandez NF, Duan Q, Wang Z, Koplev S, Jenkins SL, Jagodnik KM, Lachmann A, McDermott MG, Monteiro CD, Gundersen GW, Ma'ayan A. 2016. Enrichr: a comprehensive gene set enrichment analysis Web server 2016 update. Nucleic Acids Res 44:W90–W97. https://doi.org/10.1093/nar/gkw377.
75. Slenter DN, Kutmon M, Hanspers K, Riutta A, Windsor J, Nunes N, Melius J, Cirillo E, Coort SL, Digles D, Ehrhart F, Giesbertz P, Kalafati M, Martens M, Miller R, Nishida K, Rieswijk L, Waagmeester A, Eijssen LMT, Evelo CT, Pico AR, Willighagen EL. 2018. WikiPathways: a multifaceted pathway database bridging metabolomics to other omics research. Nucleic Acids Res 46:D661–D667. https://doi.org/10.1093/nar/gkx1064.
76. Ruepp A, Waegele B, Lechner M, Brauner B, Dunger-Kaltenbach I, Fobo G, Frishman G, Montrone C, Mewes HW. 2010. CORUM: the comprehensive resource of mammalian protein complexes—2009. Nucleic Acids Res 38:D497–D501. https://doi.org/10.1093/nar/gkp914.
77. Shannon P, Markiel A, Ozier O, Baliga NS, Wang JT, Ramage D, Amin N, Schwikowski B, Ideker T. 2003. Cytoscape: a software environment for integrated models of biomolecular interaction networks. Genome Res 13:2498–2504. https://doi.org/10.1101/gr.1239303.
78. Chatr-Aryamontri A, Ceol A, Peluso D, Nardozza A, Panni S, Sacco F, Tinti M, Smolyar A, Castagnoli L, Vidal M, Cusick ME, Cesareni G. 2009. VirusMINT: a viral protein interaction database. Nucleic Acids Res 37:D669–D673. https://doi.org/10.1093/nar/gkn739.
79. Doncheva NT, Morris JH, Gorodkin J, Jensen LJ. 2019. Cytoscape StringApp: network analysis and visualization of proteomics data. J Proteome Res 18:623–632. https://doi.org/10.1021/acs.jproteome.8b00702.
80. Kutmon M, Lotia S, Evelo CT, Pico AR. 2014. WikiPathways app for Cytoscape: making biological pathways amenable to network analysis and visualization. F1000Res 3:152. https://doi.org/10.12688/f1000research.4254.2.